1. Comparison of basin-scale *in situ* and meteoric ^{10}Be erosion and denudation rates in felsic lithologies across ~~a rainfall, slope, and~~an elevation gradient at the George River, northeast Tasmania, Australia

Leah A. VanLandingham[1], Eric W. Portenga[1], Edward C. Lefroy[2], Amanda H. Schmidt[3], Paul R. ~~Bierman[3]~~Bierman[4], Alan J. ~~Hidy[4]~~Hidy[5]

[1]Geography and Geology Department, Eastern Michigan University, Ypsilanti, MI 48197, United States
[2]Tasmanian Institute of Agriculture, University of Tasmania, Private Bag 98, Hobart 7001, Australia
~~[3]Rubenstein~~[3] Geology Department, Oberlin College and Conservatory, Oberlin, OH 44074, United States
[4]Rubenstein School for Natural Resources and the Environment, University of Vermont, Burlington, VT 05405, United States
~~[4]Center~~[5]Center for Accelerator Mass Spectrometry, Lawrence Livermore National Laboratory, Livermore, CA 94550, United States

Correspondence to: Eric W. Portenga (eric.portenga@emich.edu), Paul R. Bierman (paul.bierman@uvm.edu)

Abstract. Long-term erosion rates in Tasmania, at the southern end of Australia's Great Dividing Range, are poorly known~~.~~; yet ~~such~~, this knowledge is critical for making informed land-use decisions and improving the ecological health of coastal ecosystems. Here, we present ~~the first~~ quantitative, geologically-relevant estimates of erosion rates for the George River basin, in northeast Tasmania, based on in-situ produced ^{10}Be (^{10}Be$_i$) measured from stream sand at two trunk channel sites and seven tributaries (~~average 10.5 mm kyr~~mean 24 ~~).~~ ± 1.4 Mg km^{-2} y^{-1}; 1σ). These new ^{10}Be$_i$-based erosion rates are strongly related to elevation, which appears to control mean annual precipitation ~~rates~~ and ~~elevation, and we suggest~~temperature, but not slope, suggesting that ~~the current East-West precipitation gradient across George River greatly influences~~elevation-dependent surface processes influence rates of erosion in northeast Tasmania. This stands in contrast to erosion rates along the mainland portions of Australia's Great Dividing Range, which are ~~more strongly~~ related to basin slope. We also ~~extract~~extracted and ~~measure~~measured meteoric ^{10}Be (^{10}Be$_m$) from ~~sediment~~ grain coatings of ~~the~~sand-sized stream ~~sand~~sediment at each site, which we normalize to measured concentrations of ^{9}Be and use to estimate ^{10}Be$_m$-based ~~erosion and~~ denudation rates for the George River. ~~^{10}Be$_m$ based erosion and denudation metrics, particularly those from the central and eastern tributaries, are also closely related to elevation and precipitation in the same manner as ^{10}Be$_i$ erosion rates. Although ^{10}Be$_m$ based denudation~~ ^{10}Be$_m$-based denudation rates replicate ^{10}Be$_i$ erosion rates within a factor of two, ~~^{10}Be$_m$ based erosion rates are systematically 5–6x higher than ^{10}Be$_i$ erosion rates. ^{10}Be$_m$ erosion and denudation metrics for the westernmost headwater catchments are significantly lower than expected and have likely been affected by intensive and widespread topsoil erosion related~~but seem sensitive to recent mining, forestry, ~~which delivers large volumes of sediment rich in ^{10}Be$_m$ to tributary streams. The ^{10}Be$_i$ erosion rates presented in this study may be useful for~~and agricultural land

Formatted: Left, Numbered + Level: 1 + Numbering Style: 1, 2, 3, … + Start at: 1 + Alignment: Left + Aligned at: 0.25" + Indent at: 0.5"

Formatted: Left

Formatted: Left

Formatted: Not Superscript/ Subscript

~~managers seeking to restore ecological health~~use, all of ~~Tasmania's estuaries by reducing sediment input to levels prior to landscape~~ which resulted in widespread topsoil disturbance. Our findings suggest that $^{10}Be_m$-based denudation metrics can be used to measure landscape dynamics in geologically homogeneous landscapes where recent disturbances to topsoil profiles are minimal.

1 Introduction and the Importance of the George River, Tasmania

Erosion rates of river basins derived from measurements of the in-situ produced cosmogenic isotope, $^{10}Be_i$, have been used to ~~elucidate and~~ infer topographic, tectonic, and ~~climate~~climatic drivers of landscape evolution for thousands of individual river basins (Codilean et al., 2018; Harel et al., 2016; Mishra et al., 2019; Portenga and Bierman, 2011; Wittmann et al., 2020~~). Recently,~~) and to contextualize the effects of land use on erosion and sediment dynamics (Portenga et al., 2019; Schmidt et al., 2018). Sufficient data now exist that erosion rates from individual studies have been compiled and ~~analyzed~~analysed at the scale of entire continental orogens to demonstrate primary and secondary controls on erosion across thousands to tens of thousands of years (Aguilar et al., 2014; Carretier et al., 2018; Codilean et al., 2021; Delunel et al., 2020; Starke et al., 2020). For example, Delunel et al. (2020) find that $^{10}Be_i$ erosion rates across the European Alps are strongly linked to mean basin slope and influenced by uplift and ~~glaciations~~glaciation. A number of north-south latitudinal studies from the South American Andes show that erosion in some segments of the range ~~are~~is driven by uplift (Carretier et al., 2015; Starke et al., 2017) and slope (Carretier et al., 2018) but not necessarily rainfall unless one considers the effects of vegetation in driving soil weathering rates (Carretier et al., 2015; Starke et al., 2020).

A new compilation and analysis of $^{10}Be_i$ erosion rates across the Great Dividing Range ~~on~~of eastern Australia~~, however,~~ is the first to ~~analyze~~analyse landscape dynamics across a continent-spanning, passive, post-orogenic rift margin and finds that basin slope is most closely related to erosion at all spatial scales, more so than any other potential driver of erosion (Codilean et al., 2021). While Codilean et al.'s (2021) analysis comprises erosion rates from the ~~Western~~western and ~~Eastern~~eastern flanks of the Great Dividing Range—from tropical rainforests in northern ~~tropics~~Queensland to temperate southeast ~~Australia—~~Victoria—it is restricted to mainland Australia.

~~Here, we supplement Codilean et al.'s (2021) study~~

Despite the widespread measurement of $^{10}Be_i$ to elucidate erosion rates globally, erosion rate data do not exist for many areas of Earth's surface. Understanding of drivers of erosion will be improved by measuring erosion rates in these understudied areas. In this study, we supplement Codilean et al.'s (2021) erosion compilation with the first $^{10}Be_i$-based erosion rates from the southernmost end of the eastern Australian passive margin on the island-state of Tasmania ~~and~~, specifically the George River basin (Fig. 1). Data in this study are also the first ~~presented for~~erosion rates measured in temperate rainforests ~~in~~of the Southern Hemisphere (~~Fig. 1;~~ cf. Adams and Ehlers, 2017; Belmont et al., 2007). ~~Furthermore, important quantitative~~Quantitative erosion rate data for Tasmania and many of its fluvial systems are currently lacking (Jerie et al.,

Formatted: Left

Formatted: Left

2003; Koehnken, 2001~~), and providing new erosion rate~~); data ~~will~~, such as we provide here, are useful information for land managers and for estuary restoration efforts.

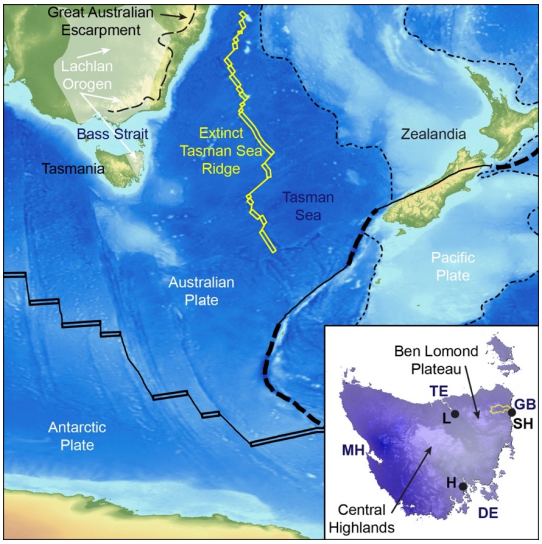

~~**Figure 1: Generalized tectonic map of the eastern Southern Ocean/southwest Pacific Ocean, surrounding Tasmania, including large-scale geologic structures in southeast Australia and Tasmania. Inset shows normalized island-wide precipitation gradient across Tasmania with darker shades of blue being areas with more precipitation. The Central Highlands establishes a pronounced rainfall shadow on the east side of the island. The Ben Lomond Plateau promotes a secondary, more-localized East-West precipitation gradient for northeast Tasmania where the field area for this study is located; the main George River basin is shown outlined in yellow. Major estuaries are indicated: Derwent Estuary (DE), Macquarie Harbour (MH), Tamar Estuary (TE), Georges Bay (GB). Cities are shown with black dots for reference: Hobart (H), Launceston (L), St. Helens (SH).**~~

~~1.1 Importance of Erosion of~~ The George River ~~and the~~empties into Georges Bay ~~Watershed~~

~~Applications of ^{10}Be, erosion studies in Australia often are set within the context of assessing the impact of sediment delivery to sensitive offshore coastal environments, primarily the Great Barrier Reef (Croke et al., 2015; Nichols et al., 2014). Recently, efforts to conserve and restore estuarine environments across Australia have gained significant traction, particularly because estuaries link terrestrial fluvial systems to coastal environments and act as a biogeochemical buffer and sediment trap between the two environments (Creighton et al., 2015; Fitzsimmons et al., 2015; Wolanski and Ducrotoy, 2014). These restoration efforts include hundreds of Tasmanian estuaries (Coughanowr and Whitehead, 2013; Edgar et al., 2000; Murphy et al., 2003), which suffer from centuries of human-caused degradation resulting from urbanization, introduction of invasive species, forestry, mining, fishing, agriculture, and tourism (Augustineus et al., 2010; Butler, 2006; Davis and Kidd, 2012; Edgar and Barrett, 2000; Ellison and Sheehan, 2014; Jones et al., 2003; Martin-Smith and Vincent, 2005; Nanson et al., 1994; Seen et al., 2004). Active conservation, restoration, and monitoring efforts are underway at many Tasmanian estuaries (Beard et al., 2008; Crawford and White, 2005; Creighton et al., 2015); none quantify geologically-relevant erosion rates nor sediment delivery, despite a recognized need to lower sediment delivery in order to reduce nutrient and pollutant loads, improve water~~

Formatted: Font color: Black

~~clarity, and prevent burial of hard surfaces important for marine life (Elliott et al., 2007; Geist and Hawkins, 2016; Noe et al., 2020; Verdonschot, 2013).~~

~~This study focuses on the Georges Bay estuary in northeast Tasmania,~~(with an 's') which is known for its oyster stocks (Mitchell et al., 2000) but has been degraded by a history of timber production, tin mining, and agriculture. Historical land-use practices in the catchment have supplied >10^6 m^3 of sediment to Georges ~~Bay's primary tributary, the George River (no "s"),~~Bay since the late 19th century (Knighton, 1991) and continue to ~~supply~~release pollutants to ~~Georges~~the Bay (Bleaney et al., 2015; Crawford and White, 2005). ~~The intensive historical industrial use of the land in the George River catchment and the threat of excess sediment delivery to the fragile estuarine environment in Georges Bay has driven state and local municipalities to focus restoration and conservation efforts on the bay. As elsewhere, the~~The success of ~~these~~ efforts to rehabilitate Georges Bay relies in part~~,~~ on reducing sediment delivery from the George River to Georges Bay to ~~Georges Bay~~pre-disturbance levels (Batley et al., 2010; Crawford and White, 2005; Kragt and Newham, 2009; McKenny and Shepherd, 1999; Mount et al., ~~2005).~~2005), but no pre-disturbance erosion data exist for the George River, nor do any geologically-relevant erosion rates exist for any part of Tasmania. Measuring erosion rates for the George River contributes to the growing geomorphological understanding of the drivers of erosion in Tasmania, across Australia, and in similar geological settings elsewhere.

1.~~2 *In*~~1 Quantifying landscape dynamics with *in* *situ* ^{10}~~Be~~ and meteoric ^{10}Be ~~erosion and denudation metrics~~

The primary goal of this study is to provide background rates (over millennia) of landscape change ~~and sediment delivery from~~in the George River ~~to Georges Bay~~basin using the *in situ* cosmogenic isotope beryllium-10 ($^{10}Be_i$) in fluvial sediment (Bierman and Steig, 1996; Brown et al., 1995; Granger et al., 1996). $^{10}Be_i$ production decreases exponentially with depth in rock and sediment ~~at~~near Earth's surface such that $^{10}Be_i$ concentrations at depths >2 m ~~is negligible~~are much lower compared to ~~that~~those measured closer to Earth's surface (Gosse and Phillips, 2001; Lal, 1991~~);~~). $^{10}Be_i$ produced by muons dominates at depths >2 m (Braucher et al., 2003; Gosse and Phillips, 2001; Heisinger et al., 1997), but muogenic $^{10}Be_i$ production is ~~generally~~ negligible when ~~compare~~compared to near-surface spallogenic $^{10}Be_i$ production, except in rapidly eroding landscapes or landscapes with steep terrain (e.g.~~,~~ Dethier et al., 2014; Fellin et al., 2017; Rosenkranz et al., 2018; Scherler et al., 2014; Siame et al., 2011~~) or in paleoerosion studies (e.g. Schaller et al., 2001, 2004, 2016).~~). Bioturbation homogenizes $^{10}Be_i$ concentrations in soils, in many places to depths of at least ~1 m (Brown et al., 1995; ~~Granger et al., 1996;~~ Schaller et al., 2018), and thus $^{10}Be_i$ erosion rates are ~~therefore considered to be~~largely insensitive to widespread shallow erosion. This insensitivity allows $^{10}Be_i$ erosion rates to be a useful gauge of pre-disturbance rates of landscape change (Ferrier et al., 2005; Portenga et al., 2019; Schmidt et al., 2018; Vanacker et al., 2007~~); exceptions have been noted~~), except where human land use is intensive (i.e.~~,~~ Schmidt et al., 2016) or the effects of human land use are exacerbated by climate extremes (i.e.~~,~~

Formatted: Font color: Auto
Formatted: Left
Formatted: Font color: Black
Formatted: Left
Formatted: Not Superscript/ Subscript

Rosenkranz et al., 2018). Pre-disturbance $^{10}Be_i$ erosion data can thus inform approaches to reducing sediment delivery from the George River and support efforts to improve the ecological health of the Georges Bay estuary and possibly other watersheds in northeast Tasmania that share similar bedrock and topographic characteristics by providing a benchmark against which to compare modern sediment loads.

Whereas In addition to $^{10}Be_i$, which is produced in rock and sediment, ^{10}Be is also produced via spallation of oxygen and nitrogen in the atmosphere; this ^{10}Be rains out or falls to Earth's surface (meteoric ^{10}Be; $^{10}Be_m$; Heikkilä and von Blanckenburg, 2015; Monaghan et al., 1986; Reusser et al., 2010a) where it is readily adsorbed into sediment grain coatings and. $^{10}Be_m$ has traditionally been used to trace sediment through landscapes (Brown et al., 1988; Heikkilä and von Blanckenburg, 2015; Helz et al., 1992; Monaghan et al., 1986; Portenga et al., 2017; Reusser et al., 2010b; Valette-Silver et al., 1986). Recently), but recently derived equations (along with a series of assumptions) now allow erosion rates and denudation rates to be calculated from measurements of $^{10}Be_m$ and the chemically similar,that are normalized to non-cosmogenic, stable ^{9}Be, which is weatheredweathers out of mineral grains ($^{9}Be_{reac}$; Willenbring and von Blanckenburg, 2010; von Blanckenburg et al., 2012). $^{10}Be_m$ erosion and $^{10}Be_m/^{9}Be_{reac}$ denudation rates have been used to quantify landscape evolution over a variety of spatial scales for long-establisheddifferent river basins ($^{10}Be_m/^{9}Be_{reac}$ denudation: Dannhaus et al., 2018; Deng et al., 2020; Harrison et al., 2021; Portenga et al., 2019; Rahaman et al., 2017; Wittmann et al., 2012, 2015); in some cases $^{10}Be_m$ is referred to as the reactive phase of $^{10}Be_m$ [$^{10}Be_{reac}$] and hasdenudation rates may be referred to as $^{10}Be_{reac}/^{9}Be_{reac}$ denudation rates) and have shown particular promise in quantifying landscape dynamics in quartz-poor landscapes (Deng et al., 2020; Rahaman et al., 2017).

Here, we consider erosion to be the physical mass loss from a landscape and denudation to be the sum of physical and chemical mass loss. Conceptually, and with regards to ^{10}Be, Portenga et al. (2019) suggested that if soil thickness approximates the zone of ^{10}Be production (<2 m) and if pH values in the environment are high (>3.9, Graly et al., 2010) such that no $^{10}Be_m$ desorbs from sediment grain coatings, erosion and denudation rates derived from measurements of $^{10}Be_i$ and $^{10}Be_m/^{9}Be_{reac}$ should be comparable and should measure landscape dynamics similarly. Although replication between $^{10}Be_i$ and $^{10}Be_m$ erosion and denudation rates at individual sites is poor (Portenga et al., 2019; Rahaman et al., 2017; Wittmann et al., 2015), average rates from $^{10}Be_i$ and $^{10}Be_m/^{9}Be_{reac}$ erosion and denudation datasets tend to be similar in magnitude, and similar spatial patterns of landscape change emerge from both $^{10}Be_i$ and $^{10}Be_m$ datasets across large regions (Deng et al., 2020; Portenga et al., 2019; Wittmann et al., 2015). Further use of the $^{10}Be_m/^{9}Be_{reac}$ denudation method in landscapes where $^{10}Be_i$ erosion can be measured and compared is important for evaluation the veracity of $^{10}Be_m$ erosion and $^{10}Be_m/^{9}Be_{reac}$ denudation calculations.

In this study, we use both $^{10}Be_i$ and $^{10}Be_m/^{9}Be_{reac}$ to measure the rates at which mass is lost from the George River basin's slopes. Over timescales sufficiently long that the assumption of steady state is approached, all of this mass will transported to

Formatted: Font color: Black

the Georges River estuary. Such mass loss form the George basin slopes is both chemical (dissolved load) and physical (sediment transport). The partitioning between these phases differs dramatically around the world depending on rock type, topography, and weathering regime and likely differs within the basin. The assumptions underlying these two methods ($^{10}Be_i$ and $^{10}Be_m$ /$^{9}Be_{reac}$) differ; results of from each method may not be the same. The concentration of $^{10}Be_i$ is biased towards mass loss within the upper meters of Earth's surface where rates of neutron spallation are high. Both chemical and physical mass losses within this surface layer of regolith are reflected by $^{10}Be_i$ concentrations. $^{10}Be_m$ /$^{9}Be_{reac}$, if the assumptions of the analytical model are met, reflects both physical and chemical mass loss throughout the regolith, regardless of depth.

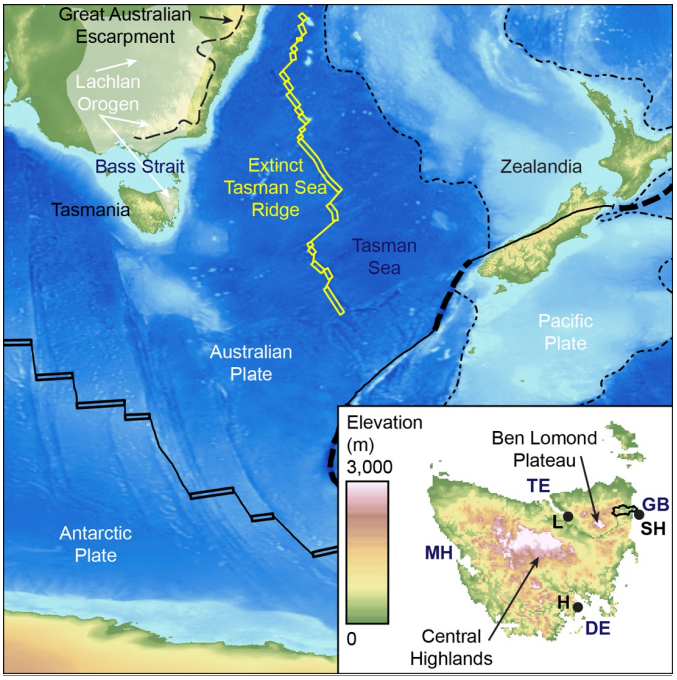

Figure 1: Generalized tectonic map of the eastern Southern Ocean/southwest Pacific Ocean, surrounding Tasmania, including large-scale geologic structures in southeast Australia and Tasmania. Inset shows detailed topography of Tasmania. The main George River basin is shown outlined in black. Major estuaries of other Tasmanian river systems are indicated for reference: Derwent Estuary (DE), Macquarie Harbour (MH), Tamar Estuary (TE), Georges Bay (GB). Cities are shown with black dots for reference: Hobart (H), Launceston (L), St. Helens (SH).

The terms "erosion" and "denudation" have been used without precision in the literature, often as a replacement for one another. Erosion is applied more often to rates calculated using the concentration of $^{10}Be_i$, while rates calculate using $^{10}Be_m$ /$^{9}Be_{reac}$ are more frequently referred to as denudation. We follow that convention in this paper. Because we have dissolved

and suspended load data as well as river flow over time from the mouth of the George River, we attempt to provide a full discussion of what the rates we measure mean for landscape dynamics within the George River Basin.

The small size and relatively uniform bedrock geology of the George River basin provide an ideal location to compare $^{10}Be_i$ erosion rates with ~~erosion and denudation rates derived using $^{10}Be_m$ and~~ $^{10}Be_m/^{9}Be_{reac}$~~, respectively (Willenbring and von Blanckenburg, 2010;~~ denudation rates (von Blanckenburg et al., 2012~~); additionally,~~). $^{10}Be_m$ can be desorbed from sediment grain coatings under high pH conditions (Aldahan et al., 1999; You et al., 1989), but $^{10}Be_m$ loss from soil profiles in solution is likely minimal in the George River basin because measured soil pH values in the catchment range from 4.0–5.5 (Kidd et al., ~~2015), thereby suggesting~~2015) and long-term monitoring of stream water pH at two gauging stations—one in Ransom Creek and the other at the George River in St. Helens—shows that ~~$^{10}Be_m$ loss to chemical weathering~~stream pH is ~~not a concern in~~consistently >5 and mostly >6 (DPIPWE, 2021a,b). The George River~~. Thus,~~ basin is a ~~secondary goal of this study is to compare $^{10}Be_m$ erosion and denudation rates to $^{10}Be_i$ erosion rates as a means of assessing the efficacy of the $^{10}Be_m$ erosion and $^{10}Be_m/^{9}Be_{reac}$ denudation methods in a landscape that minimizes~~landscape of relative geological ~~heterogeneity, which otherwise may introduce scatter to larger datasets covering larger, more~~ homogeneity in comparison to more geologically-diverse landscapes with similar data sets (i.e~~.~~., Deng et al., 2020; Portenga et al., 2019; Rahaman et al., 2017). Although the George River has a simple bedrock geology, it also has a long history of ~~intensive~~forestry and lode and placer tin mining that has, in the past, disturbed ~~its~~ the hillslopes and fluvial systems (Knighton, 1991; Preston, 2012). Given that ~~intensive~~ land~~-~~use ~~histories have~~has affected results of $^{10}Be_m$ calculations elsewhere (Portenga et al., 2019), we also explore how ~~mining~~land use in the George River affects our interpretations of ^{10}Be-based erosion and denudation calculations ~~throughout~~in this study.

Formatted: Left

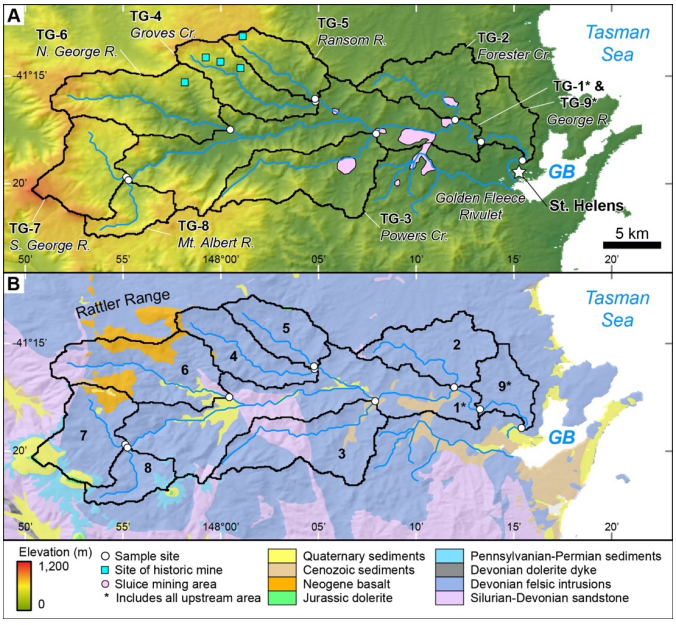

~~Figure 2: A. Shaded relief map of the topography of George River basin. Areas of historic mining are shown (Knighton, 1991), the action of which delivered >10^6 m^3 to the George River delta in Georges Bay (GB). B. Bedrock geology map of George River shows the widespread occurrence of Devonian felsic intrusions of the Blue Tier Batholith, which underlies the vast majority of the field area. Note that basins TG-2, TG-4, TG-5, and TG-8 are almost entirely underlain by~

2 Field Area

Tasmania separated from mainland Australia during Cretaceous rifting of Antarctica and Australia and sits at the southern end of the Great Australian Escarpment~~—~~—a steep arch-type escarpment that formed during the separation of Zealandia from mainland Australia in the Mid- to Late-Cretaceous (Fig. 1; Codilean et al., 2021; Crowder et al., 2019; Etheridge et al., 1987; Gaina et al., 1998; Griffiths, 1971; Gunn, 1975; Hayes and Ringis, 1973; Lanyon et al., 1993; Matmon et al., 2002; McDougall and van der Lingen, 1974; Mortimer et al., 2017; Persano et al., 2002; Sutherland et al., 2001; Weissel and Hayes, 1977). Bedrock of the George River basin ~~comprises~~is granodiorite and granite associated with the Blue Tier Batholith, which ~~were contemporaneously~~was emplaced into sediments of the Mathinna Supergroup in the Devonian (Fig. 2; Foster et al., 2000; Gee and Groves, 1971; Gray and Foster, 2004; Higgins et al., 1985; McCarthy and Groves, 1979; Seymour et al., 2006). Siluro-Devonian sedimentary rocks and Neogene basalts underlie small areas, primarily along drainage divides in the central and the western George River basin (Seymour et al., 2006).

Formatted: Font color: Black

Formatted: Left

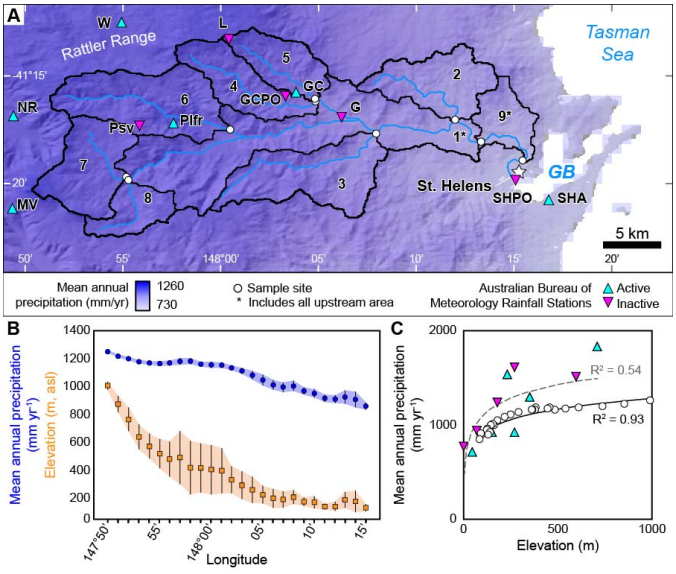

~~Figure 3: A. Mean annual precipitation across George River basin in northeast Tasmania exhibiting East-West precipitation gradient. B. Mean annual precipitation from the WorldClim global dataset (Fick and Hijmans, 2017) and elevation across George River basin binned at 01° longitudinal intervals. C. Logarithmic relationship between mean annual precipitation and elevation; data points binned at 01° longitudinal intervals. Historic rainfall data from active and inactive rainfall gaging stations (cyan and magenta triangles, respectively; BoM, 2021) is greater than modeled WorldClim rainfall for comparable elevations (Table 1), but the overall relationship between elevation and rainfall persists, regardless of which rainfall data are used.~~

The George River basin is of modest size (557 km^2) in northeastern Tasmania with low elevation (mean = 386 m) and gentle hillslopes (mean = 10~~°) that drain~~°). It drains the eastern slopes of the Rattler Range, which currently has a warm, temperate climate (Kottek et al., 2006). Despite eastern Tasmania being in the rain shadow of the central Tasmanian Highlands and western coast ranges, measurements from rainfall gauging stations and temperature data loggers within and near the George River basin show that the local topography of the Ben Lomond Plateau induces ~~a moderate east-west~~strong relationships across the basin between elevation, mean annual precipitation ~~gradient across George River basin (1,261–970 mm yr^{-1};~~, and mean annual temperature (Fig. 3; Table 1; BoM, 2021; ~~Fick and Hijmans, 2017~~Webb et al., 2018, 2020).

Formatted: Left

Table 1. Sample locations and basin data

Sample ID	Sample Location			Elevation (m)[a]	Basin Area (km^2)[a]	Relief (m)[a]	Mean weighted slope (°)[a]	Mean annual precipitation (mm yr^{-1})[b]
	River name	Latitude (°)	Longitude (°)					
TG-1	George River	-41.29017	148.22217	346	397.25	1127	10	1122
TG-2	Forester Creek	-41.27183	148.19925	141	40.21	298	6	970
TG-3	Powers Creek	-41.28286	148.13247	265	55.56	670	10	1065
TG-4	Groves Creek	-41.25514	148.08317	364	34.39	776	11	1161
TG-5	Ransom River	-41.25364	148.08239	347	27.71	709	10	1168
TG-6	North George River	-41.28067	148.00697	439	65.84	790	12	1211
TG-7	South George River	-41.32208	147.92172	652	42.53	753	9	1261
TG-8	Mt. Albert Rivulet	-41.32178	147.92592	596	20.42	631	10	1206
TG-9	George River @ St. Helens	-41.31350	148.26531	331	426.88	1174	10	1107

[a] Based or derived from Satellite Radar Topography Mission data, 90 m resolution (Gallant et al., 2011)

[b] Rainfall data are modelled precipitation rates from the WorldClim dataset, 1 km^2 resolution (Fick and Hijmans, 2017)

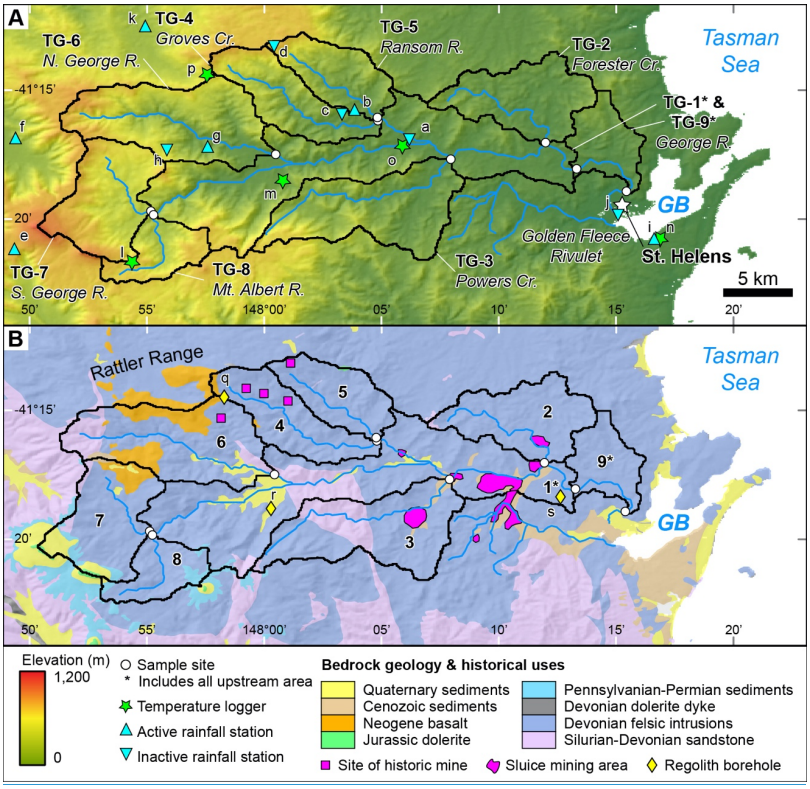

Figure 2: A. Elevation map of the topography of the George River basin. Sample collection sites (white circles), active and inactive Australian Bureau of Meteorology rainfall gauging stations (cyan triangles and cyan inverted triangles, respectively), and temperature logger locations (green stars) are shown (Webb et al., 2018, 2020). B. Bedrock geology map of George River shows the widespread occurrence of Devonian felsic intrusions of the Blue Tier Batholith, which underlies the vast majority of the field area. Note that basins TG-2, TG-4, TG-5, and TG-8 are almost entirely underlain by Devonian felsic intrusions. Areas of historic mining are shown (pink squares and polygons; Knighton, 1991), the action of which delivered >10^6 m^3 to the George River delta in Georges Bay (GB). Locations of boreholes, that strike bedrock are shown by yellow diamonds (BoM, 2015).

Human land use in Tasmania extends to >35 ka, when Aboriginal Australians crossed to ~~Tasmania~~the island from the Australian mainland ~~Australia >35 ka~~ (Cosgrove, 1995; Cosgrove et al., 1990), possibly corresponding to subaerial exposure of the Bass Strait ~56–40 ka (~~McIntosh~~MacIntosh et al., 2006) and localized ice advances in the central Tasmanian highlands (Barrows et al., 2001, 2002; ~~Macintosh~~Colhoun, 2002; MacIntosh et al., 2006). Ecological habitat suitability models, based on characteristics and locations of thousands of archaeological sites across Tasmania indicate that Aboriginal communities were located close to freshwater sources and coastal resources, such as the landscapes around Georges Bay and the lower elevations within tributaries to the George River ~~tributaries~~ (Jones et al., 2019). Human arrival in Tasmania has been linked to widespread erosion events in mid-elevation landscapes (McIntosh et al., 2009).

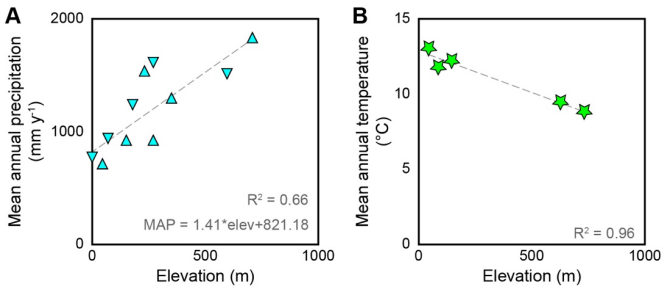

Figure 3: A. Mean annual precipitation from active (cyan triangles) and inactive (inverted cyan triangles) Australian Bureau of Meteorology rainfall gauging stations across George River basin that have at least 1 full year of recorded data exhibiting a strong correlation with station elevation. B. Mean annual temperature (green stars) taken from temperature loggers with >2 years of nearly-daily data showing a strong inverse correlation with elevation. Precipitation and temperature data shown in Table 1.

Formatted: Left

Table 1. Meteorological and Supplemental Bedrock Data for the George River Basin

Bureau of Meteorology Rainfall Station Name	Figure 2A Map ID	Bur. Of Met. Station ID	Latitude (°)	Longitude (°)	Station Elevation (m)	Data Range[a]	Years of Record	Active?	Mean Annual Precipitation (mm y^{-1})
Goshen (Post Office)	a	92065	-41.27	148.10	76	1965–1970, 1972–1973	8	No	934
Goulds Country	b	92131	-41.24	148.06	237	2005, 2016, 2018, 2020	4	Yes	1503
Goulds Country Post Office	c	92016	-41.25	148.05	183	1885–1895, 1897–1963	78	No	1228
Lottah	d	92022	-41.20	148.00	274	1902–1916, 1918–1935, 1943–1950	41	No	1611
Mt. Victoria (Una Plains)	e	91194	-41.35	147.80	710	1958, 1960, 1962–1964, 1966–1967, 1969, 1971–1974, 2011–2016, 2018–2020	21	Yes	1836
New River (New River Road)	f	91300	-41.27	147.81	274	1997, 2015, 2019–2020	4	Yes	901
Pyengana (Forest Lodge Road)	g	92051	-41.27	147.95	155	1963–1999, 2002, 2005, 2007–2008, 2010–2015, 2017–2020	51	Yes	904
Pyengana (Sea View)	h	92103	-41.28	147.92	598	1988–1992, 1994–2000, 2002, 2005–2006	15	No	1512
St Helens Aerodrome	i	92120	-41.34	148.28	48	2001, 2003–2010, 2012, 2014–2020	16	Yes	681
St Helens Post Office	j	92033	-41.32	148.25	5	1890–1904, 1906–1993, 1995–1999	108	No	777
Weldborough	k	92126	-41.18	147.90	355	2004–2011, 2013–2014, 2016	11	Yes	1265

Temperature Logger Location ID[b]	Figure 2A Map ID	Latitude (°)	Longitude (°)	Logger Elevation (m)	Data Range[b]	Years of Record	Active?	Mean Annual Temperature (°C)
1619552	l	-41.36	147.91	732	2013–2017	5	No	8.8
1620197	m	-41.30	148.01	145	2013–2017	5	No	12.2
1621107	n	-41.34	148.28	44	2013–2017	5	No	13.0
1621175	o	-41.27	148.10	86	2013–2015	3	No	11.8
2623239	p	-41.22	147.96	627	2016–2017	2	No	9.5

Depth to Regolith Borehole ID[c]	Figure 2B Map ID	Latitude (°)	Longitude (°)	Elev. of Top of Bore (m)	Depth to Bedrock through Regolith (m)
17640	q	-41.22409	147.97115	627.8	18.3
40783	r	-41.29352	148.21028	81.1	51.8
41615	s	-41.30384	148.00600	162.0	54.0

[a] Years listed in data ranges are the first and last years for which 12 months of data are available
[b] Temperature logger data sourced from the State of Tasmania Air Temperature Logger Recording Database, used by Webb et al. (2018, 2020). Each year has temperature recorded for at least 30% of days (average = 71%)
[c] Depth to regolith measured in boreholes (BoM, 2015)

Formatted: Left

Historically, decades of intensive tin lode mining in isolated headwaters of some tributaries and pockets of hydraulic sluice mining for tin in lowland floodplains introduced >10^6 m^3 of tailings to the George River and its tributaries (Fig. 2a~~), decreasing~~). Knighton (1991) notes that the pre-mining average grain-size of alluvium ~~from~~for the George River was 30–50 mm, and that this was reduced to 1–2 mm ~~(Knighton, 1991). Bedload~~during the mining era; however, it is not clear whether the 30–50 mm average grain size was specific to one sample site, or for the George River as a whole. Knighton (1991) notes that bedload characteristics have since returned to their pre-disturbance ~~levels~~values following widespread alluvium storage in floodplains and aggradation at the George River delta in Georges Bay (~~Knighton, 1991;~~ Cheetham and Martin, 2018~~).~~; Martin and Cheetham, 2018). Despite the George River's return to pre-disturbance channel and bedload characteristics, a study from an experimental forest in the Gentle Annie tributary to the George River shows that sediment yields from logged plots continue to be elevated relative to sediment yields from unlogged plots ~~continues to contribute sediment to the George River system~~ (Wilson, 1999). More recently, land use within the George River basin in 2008, at the time of sample collection, consisted primarily of forestry production from relatively natural environments and secondarily of conservation land (Fig. 4); intensive land use (i.e.~~.~~, built structures, permanent land alteration) and agricultural production from unirrigated land occur in equal proportion, though much less than the primary and secondary land uses~~;~~. Only a small percentage of the George River basin is used for agricultural production from irrigated lands (ABARES, 2016).

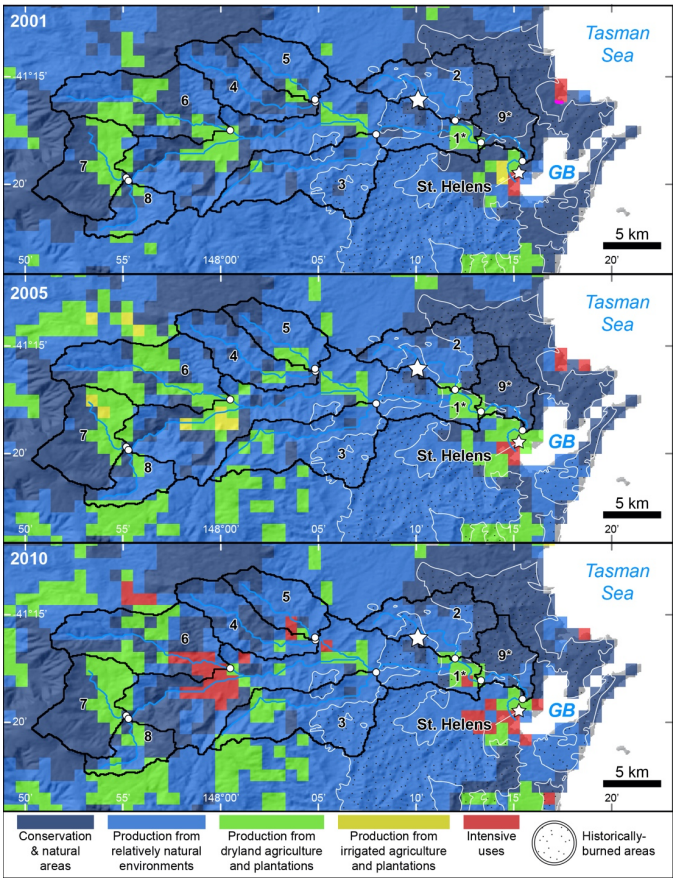

~~Figure 4: Land cover for each sampled tributary catchment in George River basin from 2001 (top), 2005 (center), and 2010 (bottom) – the period of leading up to and immediately following sample collection in 2008. The Australian Land Use and Management Classification system groups land use into five primary Classes based on their potential to impact the natural environment (ABARES, 2016). White star denotes location of the Gentle Annie experimental catchment (Wilson, 1999). Stippled areas outlined in white are areas that have been affected by forest fires or prescribed burns in the past (Land Tasmania, 2020). Asterisk (*) indicates trunk channel catchments.~~

Formatted: Font: Not Bold

Formatted: Left

3 Methods

Sediment samples for this study were collected in 2008 from several locations along the trunk (n = 2) and tributaries (n = 7) of the George River (Fig. 2; Table 2). At each site, sediment was collected from the streambed and/or in-channel bars to ensure active fluvial transport and mixing. Samples were sieved in the field to the 250–850 µm grain-size fraction. Although this grain-size is finer than the mean natural grain size (30–50 mm; Knighton, 1991), previous studies show that $^{10}Be_i$ grain-size bias is minimal or not present in small, low-elevation, low-relief, temperate landscapes where landslides are uncommon

(van Dongen et al., 2019); thus, $^{10}Be_i$ measured from the 250–850 µm grain-size fraction at George River can be interpreted as a geological erosion ~~rates. $^{10}Be_m$ and the weathered and *in situ* phases of ^9Be ($^9Be_{reac}$, $^9Be_{min}$, respectively) were measured from the 250–850 µm grain-size fraction from all seven tributary sites and one of the trunk channel sites.~~ rate.

$^{10}Be_m$ and the weathered and *in situ* phases of ^9Be ($^9Be_{reac}$, $^9Be_{min}$, respectively) were measured only from the 250–850 µm grain-size fraction from all seven tributary sites (TG-2 through TG-8) and one of the trunk channel sites (TG-9). When $^{10}Be_m$ is normalized to $^9Be_{reac}$ following von Blanckenburg et al.'s (2012) denudation rate equation, grain-size biases in resulting $^{10}Be_m/^9Be_{reac}$-based denudation rates are diminished (Wittmann et al., 2012). Singleton et al. (2016) also showed the diminishment of grain-size bias for $^{10}Be_m$ measurements when normalized to $^9Be_{reac}$. Although it is possible to calculate erosion rates from $^{10}Be_m$ alone (Harrison et al., 2021; Willenbring and von Blanckenburg, 2010), this method does not include any normalization to $^9Be_{reac}$, and $^{10}Be_m$ erosion rates are thus susceptible to grain-size bias, especially if the full grain-size distribution is not known and/or has not been analysed. As our samples are of one grain-size fraction and were collected and sieved in the field prior to $^{10}Be_m$ erosion rate derivations, we only present $^{10}Be_m/^9Be_{reac}$-based denudation rates in this study.

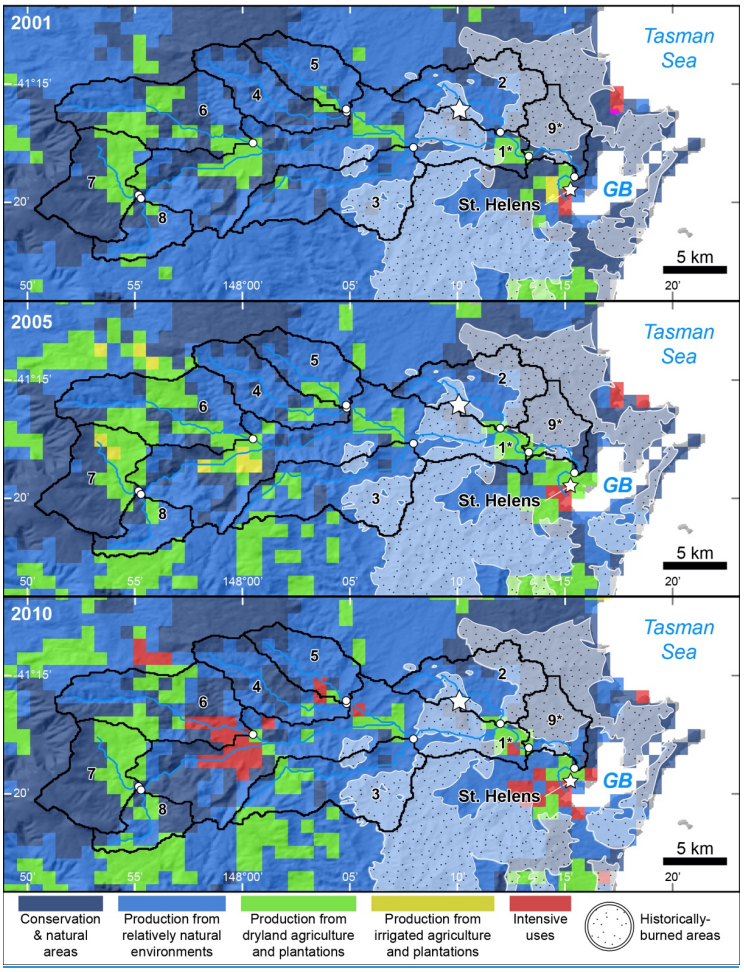

Figure 4: Land cover for each sampled tributary catchment in the George River basin from 2001 (top), 2005 (center), and 2010 (bottom) – the period of leading up to and immediately following sample collection in 2008. The Australian Land Use and Management Classification system groups land use into five primary Classes based on their potential to impact the natural environment (ABARES, 2016). White star denotes location of the Gentle Annie experimental catchment (Wilson, 1999). Stippled areas outlined in white are areas that have been affected by forest fires or prescribed burns in the past (Land Tasmania, 2020). Asterisk (*) indicates trunk channel catchments.

275

$^{10}Be_i$ was extracted at the University of Vermont from quartz from each sample ~~at the University of Vermont~~ following standard methods, during which a known amount of a ^{9}Be carrier ($^{9}Be_{carr}$) was added to each sample (Kohl and Nishiizumi, 1992; Corbett et al., 2016); relative to the amount of $^{9}Be_{carr}$, no significant native ~~beryllium~~Be was ~~detected~~found in quartz concentrates from any sample, which can otherwise lead to significant overestimates of $^{10}Be_i$-based erosion rates (Portenga et al., 2015). $^{10}Be_i/^{9}Be_{carr}$ ratios were measured by accelerator mass spectrometry at the Lawrence Livermore National Laboratory CAMS facility (Table ~~2~~3); $^{10}Be_i$ measurements were blank-corrected (the average ratio of three blanks was subtracted from the ratio of each unknown sample) and normalized to the 07KNSTD3110 AMS ^{10}Be standard material, which has a nominal $^{10}Be/^{9}Be$ ratio of 2.85×10^{-12} (Nishiizumi et al., 2007). $^{10}Be_i$ production was averaged across all sampled basins to a single point following Portenga and Bierman (2011), and the ~~CRONUS-on-line~~online erosion rate calculator ~~(~~described by Balco et al.~~,~~ (2008~~)~~), which has been subsequently updated, was used to derive $^{10}Be_i$ erosion rates following the Lal (1991) and Stone (2000) scaling schemes (ε, ~~Table 3); here~~Tables 4, 5). Here, ε is presented in units of ~~mm kyr^{-1}. As in Portenga et al. (2019), we present ^{10}Be$_i$-based sediment flux rates in this study (Appendix A), which we present as the factor of ε and ρ in units of~~ Mg km^{-2} ~~yr^{-1}, so as~~ky^{-1} (Table 5) allowing us to compare ~~to~~measures of ε directly with $^{10}Be_m/^{9}Be_{reac}$-based denudation rates (D_m; see below). Muogenic production of $^{10}Be_i$ is incorporated into ~~^{10}Be$_i$-based erosion rates~~ε; however, muogenic $^{10}Be_i$ is negligible relative to spallogenic $^{10}Be_i$ production given the George River's post-orogenic, low-elevation, low-relief setting.

Formatted: Left

Formatted: Strikethrough

Table 2. Isotope data

In situ Sample ID	UVM Batch No.	Quartz mass (g)	Carrier mass (µg)	LLNL Sample ID	$^{10}Be_i/^{9}Be_{carr}$	± 1σ	$^{10}Be_i$ (atoms g^{-1})	± 1σ
TG-1	432[a]	20.099	250.791	BE28820	4.37E-13	7.83E-15	3.64E+05	6.52E+03
TG-2	438[b]	20.100	249.506	BE29129	6.83E-13	9.31E-15	5.66E+05	7.72E+03
TG-3	438	22.423	249.704	BE29130	4.79E-13	1.41E-14	3.97E+05	1.17E+04
TG-4	438	19.288	248.814	BE29131	3.10E-13	8.41E-15	2.56E+05	6.95E+03
TG-5	438	20.702	250.296	BE29133	4.37E-13	1.02E-14	3.63E+05	8.48E+03
TG-6	446[c]	20.532	249.209	BE29303	2.81E-13	6.11E-15	2.33E+05	5.05E+03
TG-7	446	20.156	249.111	BE29304	2.28E-13	6.76E-15	1.88E+05	5.60E+03
TG-8	446	20.747	249.704	BE29305	2.99E-13	7.35E-15	2.48E+05	6.10E+03
TG-9	446	20.169	250.791	BE29306	4.94E-13	1.19E-14	4.11E+05	9.92E+03

Meteoric Sample ID	UVM Batch No.	Sample mass (g)	Carrier mass (µg)	LLNL Sample ID	$^{10}Be_m/^{9}Be_{carr}$	± 1σ	Q toms cm^{-2} yr	$^{10}Be_{met}$ (atoms g^{-1})	± 1σ	$^{9}Be_{min}$ (atoms g^{-1})	$^{9}Be_{reac}$ (atoms g^{-1})
TG-2	MB-15[d]	0.463	328.71	BE27783	1.51E-12	2.07E-14	8.12E+05	7.16E+07	9.83E+05	2.51E+16	1.32E+16
TG-3	MB-15	0.497	298.02	BE27784	1.50E-12	2.26E-14	8.92E+05	5.99E+07	9.05E+05	3.19E+16	1.06E+16
TG-4	MB-15	0.457	296.04	BE27785	1.12E-12	1.55E-14	9.73E+05	4.84E+07	6.69E+05	3.29E+16	1.08E+16
TG-5	MB-15	0.491	300.00	BE27786	1.05E-12	1.46E-14	9.79E+05	4.29E+07	5.95E+05	2.84E+16	1.09E+16
TG-6	MB-15	0.466	300.99	BE27787	4.30E-12	5.79E-14	1.01E+06	1.85E+08	2.50E+06	4.54E+16	4.06E+16
TG-7	MB-15	0.487	299.01	BE27788	5.60E-12	6.09E-14	1.06E+06	2.30E+08	2.50E+06	3.09E+16	5.82E+16
TG-8	MB-15	0.487	300.00	BE27789	5.35E-12	5.83E-14	1.01E+06	2.20E+08	2.40E+06	2.71E+16	5.54E+16
TG-9	MB-15	0.541	299.01	BE27790	1.19E-12	1.64E-14	9.28E+05	4.39E+07	6.06E+05	1.53E+16	1.08E+16

[a] In situ Batch 432 Blank $^{10}Be_i/^{9}Be_{carr}$ ratio = $1.25 \times 10^{-14} \pm 5.87 \times 10^{-16}$
[b] In situ Batch 438 Blank $^{10}Be_i/^{9}Be_{carr}$ ratio = $1.22 \times 10^{-14} \pm 1.82 \times 10^{-15}$
[c] In situ Batch 446 Blank $^{10}Be_i/^{9}Be_{carr}$ ratio = $1.27 \times 10^{-14} \pm 6.70 \times 10^{-16}$
[d] Meteoric Batch MB-15 Blank $^{10}Be_m/^{9}Be_{carr}$ ratio = $1.65 \times 10^{-14} \pm 1.72 \times 10^{-15}$

Table 3. Erosion and denudation rates

Sample ID	ε [a] (mm kyr^{-1})	± 2σ	Integration duration (kyr)	Sed Flux (Mg km^{-2} yr^{-1})	± 2σ	E (mm kyr^{-1})	± 2σ	D_m (Mg km^{-2} yr^{-1})	± 2σ
TG-1	9.6	1.6	61.8	25.9	4.3				
TG-2	4.8	0.8	122.5	13.1	2.2	42.8	0.6	26.0	0.7
TG-3	8.1	1.4	73.7	21.7	3.8	56.2	0.8	37.9	1.1
TG-4	14.1	2.4	42.1	38.1	6.5	75.9	1.0	52.6	1.5
TG-5	9.6	1.6	62.0	25.8	4.4	86.1	1.2	53.7	1.5
TG-6	16.7	2.8	35.5	45.1	7.5	20.7	0.3	28.2	0.8
TG-7	24.5	4.2	24.2	66.2	11.3	17.4	0.2	24.5	0.5
TG-8	17.6	3.0	33.7	47.5	8.0	17.3	0.2	22.7	0.5
TG-9	8.3	1.4	71.5	22.4	3.8	79.8	1.1	33.0	0.9

[a] ^{10}Be$_i$ erosion rates calculated using the CRONUS erosion rate calculator version 3.0, wrapper version 3.0 erates version 3.0, muons version 3.1 (Balco et al., 2008)

^{10}Be$_m$ was extracted following Stone's (1998) fusion method and a ^{9}Be carrier solution was added to each sample. Through this process, some amount of ^{10}Be$_i$ from bulk sediment is incorporated into the ^{10}Be$_m$ sample; however, the amount of ^{10}Be$_i$ is negligible, consistently two orders of magnitude less than ^{10}Be$_m$ measurements (Table 3). ^{10}Be$_m$/^{9}Be$_{carr}$ ratios of these fusion extracts were measured at the Lawrence Livermore National Laboratory CAMS facility, blank-corrected (ratio of one blank was subtracted from ratio of each unknown ~~samples~~sample; Table ~~2~~3) and normalized to the 07KNSTD3110 standard material (Nishiizumi et al., 2007). Sample material used to calculate ^{9}Be$_{reac}$ was first subject to ~~strong~~6N HCl acid leaching to remove sediment grain coatings (Greene, 2016; Portenga et al., 2019 supplement); it was then fully digested in HF and ^{9}Be$_{min}$ was measured in that solution. Both ^{9}Be$_{reac}$ from sediment grain coatings and ^{9}Be$_{min}$ from the remaining mineral material were measured by inductively coupled plasma-optical emission spectrometry (ICP-OES) at the University of Vermont. ~~In this study, E and D_m are presented in units of mm kyr^{-1} and Mg km^{-2} yr^{-1}, respectively.~~Together, these data were used to derive denudation rates following von Blanckenburg et al. (2012; Table 4). At the time of sample collection (2008), the equations to calculate D_m had not been published, and bedrock samples from the field area were not collected. We therefore rely on using a global crustal average of 2.5 ppm for the amount of native ^{9}Be in our samples (von Blanckenburg et al., 2012). In this study, D_m is presented in units of Mg km^{-2} y^{-1} (Table 5).

~~E and D_m presented in this study (Table 3) are calculated using values of Q that range from 8.12 x 10^{5} atoms cm^{-2} yr^{-1} to 1.06 x 10^{6} atoms cm^{-2} yr^{-1} (Appendix A; Graly et al., 2011). Values of Q used here are of the same order of magnitude as ^{10}Be$_m$ accumulation rates measured from a similar latitude in New Zealand (1.68 to 1.72 x 10^{6} atoms cm^{-2} yr^{-1}; Reusser et al., 2010a), those integrated throughout the Holocene (1.0–1.5 x 10^{6} atoms cm^{-2} yr^{-1}; Heikkilä and von Blanckenburg, 2015), and atmospheric-depth integrated rates of Q (~7 x 10^{5} atoms cm^{-2} yr^{-1}; Masarik and Beer, 2009; Willenbring and von Blanckenburg, 2010). We choose to use Graly et al.'s (2011) approach to deriving values of Q for this study since they are specific to the latitude and rainfall for each basin.~~

Values for the rate at which ^{10}Be$_m$ is delivered from the atmosphere to Earth's surface ($^{10Be}F_{met}$) have been measured and modelled in various ways at both local and global scales, each with its own strengths. For instance, in the southwest Pacific

Formatted: Not Superscript/ Subscript

Formatted: Left

Formatted: Font: Not Italic, Superscript

region, Reusser et al. (2010a) directly measured $^{10Be}F_{met}$ in a dated New Zealand paleosol (1.68 to 1.72 x 10^6 atoms cm^{-2} y^{-1}). In the absence of direct measurement, $^{10Be}F_{met}$ must be estimated or modelled. Heikkilä and von Blanckenburg integrate $^{10Be}F_{met}$ through the Holocene while others integrate $^{10Be}F_{met}$ for total atmospheric thickness, all at a global scale (Masarik and Beer, 2009; Willenbring and von Blanckenburg, 2010), but the resolution of these models is not fine-enough for the small spatial scale of this study, and $^{10Be}F_{met}$ would be the same for each sampled basin (1.0–1.5 x 10^6 atoms cm^{-2} y^{-1} for Holocene integrated or ~7 x 10^5 atoms cm^{-2} y^{-1} for atmospheric depth-integrated $^{10Be}F_{met}$). Graly et al. (2011), however, present an equation that estimates $^{10Be}F_{met}$ from a location's mean annual precipitation and latitude, which provides a more specific value for $^{10Be}F_{met}$ for any selected study site. Here, we use estimated values of $^{10Be}F_{met}$ based on Graly et al.'s (2011) model because it provides an estimate of $^{10Be}F_{met}$ that is specific for each sampled basin in this study; these values range from 8.55 x 10^5 atoms cm^{-2} y^{-1} to 1.46 x 10^6 atoms cm^{-2} y^{-1}, which are of the same order of magnitude as $^{10Be}F_{met}$ measured in New Zealand (Reusser et al., 2010a) or those based on global $^{10Be}F_{met}$ models (Heikkilä and von Blanckenburg, 2015; Masarik and Beer, 2009; Willenbring and von Blanckenburg, 2010). We use mean annual precipitation values calculated from our own correlation of gauging stations against elevation (Figure 3A) because of inconsistencies, described below, between measured data and modelled data in our study area.

Table 2. Sample locations and topographical basin data

Sample ID	Sample Location			Basin-average elevation (m)[a]	Basin Area (km^2)[a]	Mean local relief (m)[a]	Mean Basin slope (°)[a]	Mean Annual Precipitation (mm y^{-1})[b]	% of Tributary with >"High" Erosivity[c]
	River name	Latitude (°)	Longitude (°)						
TG-1	George River	-41.29017	148.22217	346	397.25	218.0	10	1,310	
TG-2	Forester Creek	-41.27183	148.19925	141	40.21	120.0	6	1,020	9.2
TG-3	Powers Creek	-41.28286	148.13247	265	55.56	214.8	10	1,195	38
TG-4	Groves Creek	-41.25514	148.08317	364	34.39	238.0	11	1,336	49.5
TG-5	Ransom River	-41.25364	148.08239	347	27.71	226.8	10	1,312	48.8
TG-6	North George River	-41.28067	148.00697	439	65.84	275.5	12	1,442	49.3
TG-7	South George River	-41.32208	147.92172	652	42.53	211.5	9	1,743	26.9
TG-8	Mt. Albert Rivulet	-41.32178	147.92592	596	20.42	227.8	10	1,663	40.4
TG-9	George River @ St. Helens	-41.31350	148.26531	331	426.88	213.5	10	1,289	

[a] Based or derived from Satellite Radar Topography Mission data, 90 m resolution (Gallant et al., 2011). Mean local relief calculated using a 10-cell (~900 m) circular moving window.
[b] Used in the calculation of the meteoric ^{10}Be delivery rate, $^{10Be}F_{met}$, for each catchment (Graly et al., 2011). Calculated using the basin average elevation and using the regression equation betwee and mean annual precipitation at Australian Bureau of Meteorology stations (Figures 2, 3; Table 1).
[c] Erosivity ratings from Kidd et al. (2014, 2015).

Table 3. Isotope data

In situ Sample ID	UVM Batch No.	Quartz mass (g)	Carrier mass (µg)	LLNL Sample ID	$^{10}Be_i/^9Be_{carr}$	± 1σ	$^{10}Be_i$ (atoms g^{-1})	± 1σ
TG-1	432[a]	20.099	250.791	BE28820	4.37E-13	7.83E-15	3.64E+05	6.52E+03
TG-2	438[b]	20.100	249.506	BE29129	6.83E-13	9.31E-15	5.66E+05	7.72E+03
TG-3	438	22.423	249.704	BE29130	4.79E-13	1.41E-14	3.97E+05	1.17E+04
TG-4	438	19.288	248.814	BE29131	3.10E-13	8.41E-15	2.56E+05	6.95E+03
TG-5	438	20.702	250.296	BE29133	4.37E-13	1.02E-14	3.63E+05	8.48E+03
TG-6	446[c]	20.532	249.209	BE29303	2.81E-13	6.11E-15	2.33E+05	5.05E+03
TG-7	446	20.156	249.111	BE29304	2.28E-13	6.76E-15	1.88E+05	5.60E+03
TG-8	446	20.747	249.704	BE29305	2.99E-13	7.35E-15	2.48E+05	6.10E+03
TG-9	446	20.169	250.791	BE29306	4.94E-13	1.19E-14	4.11E+05	9.92E+03

Meteoric Sample ID	UVM Batch No.	Sample mass (g)	Carrier mass (µg)	LLNL Sample ID	$^{10}Be_m/^9Be_{carr}$	± 1σ	$^{10Be}F_{met}$ (atoms cm^{-2} y^{-1})	$^{10}Be_m$ (atoms g^{-1})	± 1σ	$^9Be_{min}$ (atoms g^{-1})	$^9Be_{reac}$ (atoms g^{-1})
TG-2	MB-15[d]	0.463	328.71	BE27783	1.51E-12	2.07E-14	8.12E+05	7.16E+07	9.83E+05	2.51E+16	1.32E+16
TG-3	MB-15	0.497	298.02	BE27784	1.50E-12	2.26E-14	8.92E+05	5.99E+07	9.05E+05	3.19E+16	1.06E+16
TG-4	MB-15	0.457	296.04	BE27785	1.12E-12	1.55E-14	9.73E+05	4.84E+07	6.69E+05	3.29E+16	1.08E+16
TG-5	MB-15	0.491	300.00	BE27786	1.05E-12	1.46E-14	9.79E+05	4.29E+07	5.95E+05	2.84E+16	1.09E+16
TG-6	MB-15	0.466	300.99	BE27787	4.30E-12	5.79E-14	1.01E+06	1.85E+08	2.50E+06	4.54E+16	4.06E+16
TG-7	MB-15	0.487	299.01	BE27788	5.60E-12	6.09E-14	1.06E+06	2.30E+08	2.50E+06	3.09E+16	5.82E+16
TG-8	MB-15	0.487	300.00	BE27789	5.35E-12	5.83E-14	1.01E+06	2.20E+08	2.40E+06	2.71E+16	5.54E+16
TG-9	MB-15	0.541	299.01	BE27790	1.19E-12	1.64E-14	9.28E+05	4.39E+07	6.06E+05	1.53E+16	1.08E+16

[a] In situ Batch 432 Blank $^{10}Be_i/^9Be_{carr}$ ratio = 1.25 x 10^{-14} ± 5.87 x 10^{-16}
[b] In situ Batch 438 Blank $^{10}Be_i/^9Be_{carr}$ ratio = 1.22 x 10^{-14} ± 1.82 x 10^{-15}
[c] In situ Batch 446 Blank $^{10}Be_i/^9Be_{carr}$ ratio = 1.27 x 10^{-14} ± 6.70 x 10^{-16}
[d] Meteoric Batch MB-15 Blank $^{10}Be_m/^9Be_{carr}$ ratio = 1.65 x 10^{-14} ± 1.72 x 10^{-15}

We compare ε, ~~sediment flux, E,~~ and D_m to various topographic and ~~climatic~~land-use factors to assess ~~dominant~~possible processes driving or related to background landscape evolution in the George River (~~Table~~Tables 1, 2). Topographic data are derived from the SRTM 90-m resolution global dataset (Gallant et al., 2011). ~~We use mean annual precipitation data from the updated WorldClim global dataset instead of precipitation from meteorological stations because of its greater spatial coverage, but we note that while WorldClim rainfall values are nominally lower than measured~~ Mean local relief was calculated over a moving 10-cell (~900 m) circular window. We do not compare ε or D_m to climate data from global gridded datasets for mean annual temperature and mean annual precipitation, although such data are available. This is because the gridded datasets are all models based on limited measurements and include a strong elevation component in their interpolation scheme (e.g. WorldClim, Fick and Hijmans, 2017) or have spatial resolutions that do not provide sufficient detail for the small size of the George River basin (e.g. TRMM, Huffman, 2021). These characteristics of gridded climate datasets makes it difficult to attribute erosion to climatic drivers independent of their self-correlation with elevation. Thus, we rely on observed relationships between elevation and precipitation and temperature data from precipitation gauges (n = 10, each with >4 years of daily data; Table 1, Figs. 2, 3) and temperature loggers (n = 5, each with >2 years of hourly data from at least 30% of days reporting [average = 70% of days reporting]; Table 1, Figs. 2, 3). Although the spatial coverage of rainfall gauges and temperature loggers is small relative to the coverage of interpolated, modelled, gridded data, they provide us an opportunity to work with real measured data

Table 4. Erosion and Denudation Rate Equations

Equation	Variable	Description	Unit
	ε	$^{10}Be_i$ erosion rate	cm y^{-1}
$^{10}Be_i$: Erosion Rate	Λ	Attenuation length for cosmic-ray penetration[a]	160 g cm^{-2}
	P_0	Production rate of $^{10}Be_i$ at Earth's surface[b]	atoms g^{-1} y^{-1}
$\varepsilon = \Lambda\left(\frac{P_0}{N} - \lambda\right)$	N	Measured concentration of *in-situ* produced $^{10}Be_i$	atoms g^{-1}
	λ	^{10}Be decay constant[c]	y^{-1}
	Q	Atmospheric $^{10}Be_m$ delivery rate	atoms cm^{-2} y^{-1}
$^{10}Be_m$ / $^9Be_{eac}$ Denudation Rate[d]	$^{10}Be_m$	Measured concentration of $^{10}Be_m$ extracted from sediment grain coatings	atoms g^{-1}
	D_m	$^{10}Be_m/^9Be_{eac}$-based denudation rate	g cm^{-2} y^{-1}
$D_m = \frac{Q\left(\frac{^9Be_{min}}{^9Be_{reac}} + 1\right)}{\left(\frac{^{10}Be_m}{^9Be_{reac}}\right) {}^9Be_{parent}}$	$^9Be_{min}$	Measured concentration of ^9Be still within mineral grains	atoms g^{-1}
	$^9Be_{reac}$	Measured concentration of ^9Be extracted from sediment grain coatings	atoms g^{-1}
	$^9Be_{parent}$	Assumed concentration of ^9Be in crustal bedrock[e]	1.671 x 10^{17} atoms g^{-1}

[a] Balco et al. (2008), Gosse and Phillips (2001)
[b] Scaled for each basin following Lal (1991) and Stone (2000)
[c] Half-life of ^{10}Be = 1.36 My
[d] von Blanckenburg et al. (2012)
[e] Derived from an assumed value of 2.55 ppm, following von Blanckenburg et al. (2012)

Table 5. *In Situ* ^{10}Be Erosion Rates and Meteoric ^{10}Be Denudation Rates

Sample ID	$^{10}Be_i$ erosion, ε[a] (Mg km^{-2} y^{-1})	± 1σ[a]	Integration duration (ky)	$^{10}Be_m/^9Be_{eac}$ denudation rate, D_m (Mg km^{-2} y^{-1})	± 1σ
TG-1	25.9	2.2	61.8		
TG-2	13.1	1.1	122.5	27.4	0.4
TG-3	21.7	1.9	73.7	42.5	0.6
TG-4	38.1	3.2	42.1	60.5	0.8
TG-5	25.8	2.2	62.0	60.3	0.8
TG-6	45.1	3.8	35.5	33.6	0.5
TG-7	66.2	5.7	24.2	33.9	0.4
TG-8	47.5	4.0	33.7	31.3	0.3
TG-9	22.4	1.9	71.5	38.4	0.5

[a] $^{10}Be_i$ erosion rates calculated using the CRONUS erosion rate calculator version 3.0, wrapper version 3.0, erates version 3.0, muons version 3.1 (Balco et al., 2008).

Proper interpretation of $^{10}Be_m$ derived denudation rates requires an understanding of the potential for beryllium weathering and desorption from sediment grain coatings and mobility through regolith (von Blanckenburg et al., 2012). To this end, information on (1) the depth of regolith and (2) chemical weathering data across the George River basin are needed. A potentially relevant dataset available for Tasmania is an interpolated gridded map of depth of regolith (Wilford et al., 2016). However, like the WorldClim precipitation and temperature datasets, the gridded regolith dataset was created by interpolating measured data from around Australia using a model and has an implicit dependence on elevation that does not reflect measured depths to bedrock in the George River basin. Only three boreholes exist in the George River basin that clearly go through regolith to bedrock, from which we extracted regolith depth (BoM, 2015; Fig. 2A; Table 1). They do not match the model results. These three boreholes, and others in the study area, have some units that could be alluvium or regolith; this differentiation is not clear and therefore the depth of regolith could be overestimated if alluvium is marked as regolith. Thus, we cannot know with certainty the depth of regolith across our field area and we therefore cannot draw any clear conclusions about beryllium mobility in deep, weathered soils from the borehole data alone and do not explore it further.

There is one long term water quality and stream gauging station in the George River basin. It is at the inlet to the local water treatment plant for the trunk channel of the George River in the town of St. Helens (Fig. 2). Thus, we can only estimate the degree of chemical weathering for the entire George River basin, not individual tributaries. Chemical weathering rates for the George River at St. Helens were calculated using water quality data (i.e., dissolved major and trace element data) and

discharge data (J. Fawcett, TasWater, pers. comm. 2021). ~~both datasets show increased rainfall at higher elevations (Fig. 3c; BoM, 2021). Ratings of soil erosivity have been derived~~ Discharge measurements were taken at intervals ranging from 4 to 96 times per day from 1968 to 2021; 26 complete years of discharge data were available. Water quality measurements have been conducted since 2015 and we used the data from July 2015 to September 2021 in our derivation of chemical weathering for the George River basin. We matched water quality measurements with the nearest discharge measurement in time; when times did not line up exactly, we used the average of the nearest two discharge measurements (Table 6). We then explored the relationship between discharge and each water quality parameter. For parameters that are invariant with discharge (iron, potassium, sulphate, silica), we calculated the mean concentration of the parameter. For parameters that scale with discharge (calcium, magnesium), we used a rating curve to determine how discharge relates to each water quality parameter; we then applied the mean measured values and rating curves, as appropriate, to every discharge measurement for years with complete discharge records. Sodium and chlorine were balanced (suggesting a sea salt contribution) and were thus omitted from the calculation. Carbonate that balanced the calcium and magnesium present was included; the rest was assumed to be from atmospheric sources. Silica concentrations were measured independently, once annually from 1974 to 1981 (J. Fawcett, TasWater, pers. comm. 2021), and we used all eight of those measurements; measurements in individual years were taken in March, June, August, October, and November. We report total dissolved solids (TDS) measurements that are the sum of potassium, sulphate, silica, calcium, magnesium, and carbonate concentrations following West et al. (2005)'s chemical weathering rate calculation. We used a similar method to calculate the total suspended sediment (TSS) for each year of complete discharge data; TSS scales with discharge and so we applied a rating curve.

Formatted: Font: 10 pt, Not Bold

Table 6. Water Quality Data for the George River at St. Helens

Parameter	Number of Datapoints	Calculation technique	Equation used	Mean value [ppm]
Iron	25	Mean value		0.45
Potassium	24	Mean value		1.03
Sulphate	24	Mean value		2.03
Silica	8	Mean value		9.90
Calcium	24	Rating curve	-0.06 * Discharge + 0.90	
Magnesium	24	Rating curve	-0.045 * Discharge + 0.55	
Carbonate		Required to balance Ca and Mg	1.5*Ca+2.5*Mg	
Total suspended solids	25	Rating curve	0.66 * Discharge + 0.25	

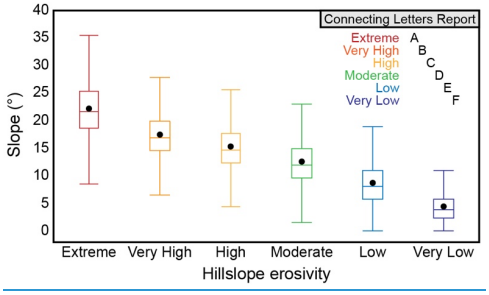

Figure 5: Analysis of variance, showing hillslope angles associated with categories of landscape erosivity (Kidd et al., 2014, 2015) at George River. Box-and-whiskers cover ±1.5x the interquartile range; black dot is the mean slope for the erosivity category. The mean slope for each erosivity category is significantly different from every other category, illustrated by the Connecting Letters Report (if the mean slope in any two erosivity categories were statistically indistinguishable, they would otherwise share a letter in the report). We therefore use hillslope angle as a quantitative proxy for erosivity in the George River basin.

Lastly, qualitative ratings of soil erosivity have previously been determined for Tasmania (Kidd et al., 2014, 2015) ~~and~~based on modelled soil loss should substantial vegetation and ground cover be removed; these ratings are strongly tied to hillslope angle within ~~George River basin (Fig. 5); thus, comparing~~the George River basin (Fig. 5). Additionally, slope and erosion are strongly linked across the Great Dividing Range on the Australian mainland (Codilean et al., 2021). Thus, we compare erosion and denudation metrics against basin slope metrics ~~provides an adequate assessment of whether models~~ , which enables us to compare our measures of ε and D_m to basin slope to assess how Kidd et al.'s (2014, 2015) metrics for of hillslope erodibility ~~influences~~and erosion in the George River are related and to compare these new $^{10}Be_i$ erosion rates to those presented by Codilean et al. (2021) for the Australian mainland.

4 Results

4.1 $^{10}Be_i$ erosion rates, ε

Erosion rates, ε, based on measured concentrations of ~~in situ ^{10}Be (Table 3)~~ $^{10}Be_i$ range from ~~4.8~~13.1 to ~~24.5 mm kyr^{-1} (Appendix A), and we find that the average~~ 66.2 Mg km^{-2} y^{-1}. They integrate landscape dynamics in the George River basin since ~24–122 ka (Table 4). The average ε from tributaries (~~13.6 ± 1.0 mm kyr^{-1}~~ 36.8 ± 1~~; 2σ~~.3 Mg km^{-2} y^{-1}) is greater than from either of the trunk channel samples (TG-1 = 25.9~~.6 ± 1.6 mm kyr^{-1}~~ ± 2.2 Mg km^{-2} y^{-1}; TG-9 = ~~8.3~~22.4 ± 1.~~4 mm kyr^{-1}~~9 Mg km^{-2} y^{-1}~~; 2σ~~). Tributary values for ε~~, and ε-based sediment flux rates~~ are greater in the high-elevation, western headwaters of the George River basin and decrease systematically, eastwards towards the lower-elevation coast (Fig. ~~6). This eastward decrease in ε also corresponds to a decrease in rainfall along the precipitation gradient (~~6; R^2 = 0.~~82); relationships~~91, $p < 0.001$). Relationships between ε in tributary catchments and ~~basin~~mean local relief, mean basin ~~weighted~~ slope, and the percent of each basin that is categorized as being greater than or equal to "High" Erosivity are weak ~~(Fig. 7;~~ and not significant (R^2 = 0.~~39~~28, R^2 = 0.17, R^2 = 0.05, respectively~~).~~

, $p \geq 0.13$). Taking the product of ε and ~~the~~basin area ~~of each catchment~~ provides us with the average annual ~~volume of sediment exported from~~mass loss for each catchment. Making the assumption of steady state and no change in storage over ~~millennia. Summing these volumes, shows that a similar volume of sediment~~ time, we can then compare mass export rates across the catchment. Following this approach, we find that a similar mass exited sampled tributaries (10,511 ± 394 Mg y^{-1}) as the mass that passes through the trunk channel ~~sample~~ sites ~~annually as the sum of sediment exiting sampled tributaries (~~(TG-1 = ~~3.8 ± 0.7 km^2 yr~~10,286 ± 859 Mg y^{-1}; TG-9 = ~~3.5 ± 0.7 km^2 yr^{-1}; tributaries = 3.9 ± 0.3 km^2 yr~~9,555 ± 817 Mg y^{-1}~~; 2σ). Trunk channel samples, TG-1 and TG-9, should also incorporate erosion~~). This comparison suggests little to no contribution of mass from ~~their respective subcatchments – the area upstream of~~ the ~~sample site, but downstream of all tributary sample points. Using regression equations for ε and longitude, elevation, and precipitation, each, an average modelled ε for TG-1 is 9.6 ± 3.0 mm kyr^{-1} and an average modelled ε for TG-9 is 1.1 ± 3.1 mm kyr^{-1}. The average volume of~~

Formatted: Left

Formatted: Not Superscript/ Subscript

Formatted: Font: Bold

Formatted: Not Superscript/ Subscript

Formatted: Left

~~sediment these subcatchments contribute to annual sediment loads, based on modelled *c* data are TG-1 = 1.1 ± 0.4 km^3 yr^{-1} and TG-9 = 0.0 ± 0.1 km^3 yr^{-1}~~lowland, mainstem George River valley below the tributaries and above the basin outlet sampling sites.

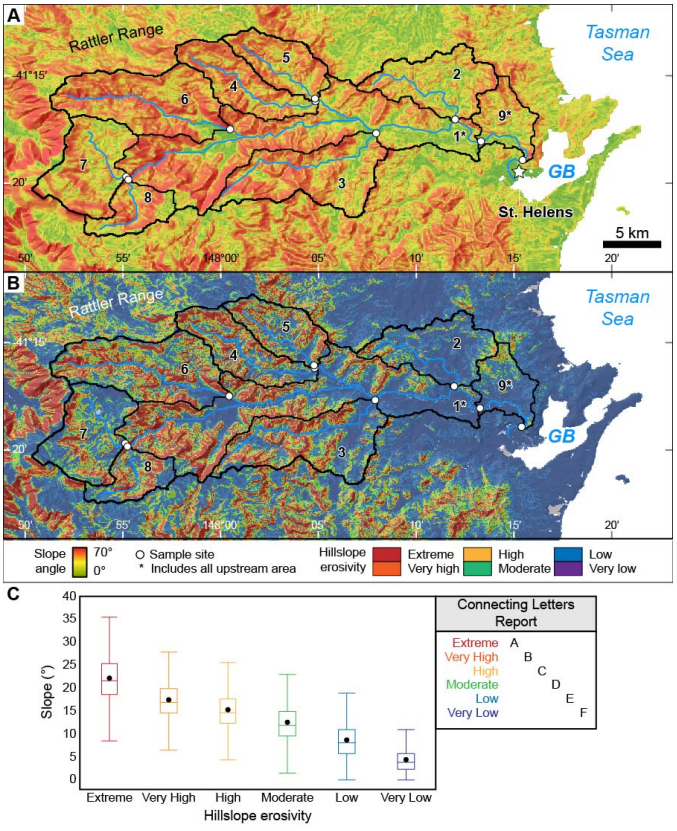

~~**Figure 5: A. Map of hillslope angle across George River basin, derived from 90 m SRTM digital elevation models. B. Map of hillslope erosivity across George River basin, from Kidd et al. (2014, 2015). C. Analysis of variance, showing hillslope angles associated with categories of landscape erosivity (Kidd et al., 2014, 2015) at George River. Box-and-whiskers cover ±1.5x the interquartile range; black dot is the mean slope for the erosivity category. Comparison of means for each category indicate that the means of erosivity categories are all significantly different from each other (i.e. no categories are linked by the same letter in the Connecting Letters Report); we use hillslope angle as a quantitative proxy for erosivity at George River.**~~

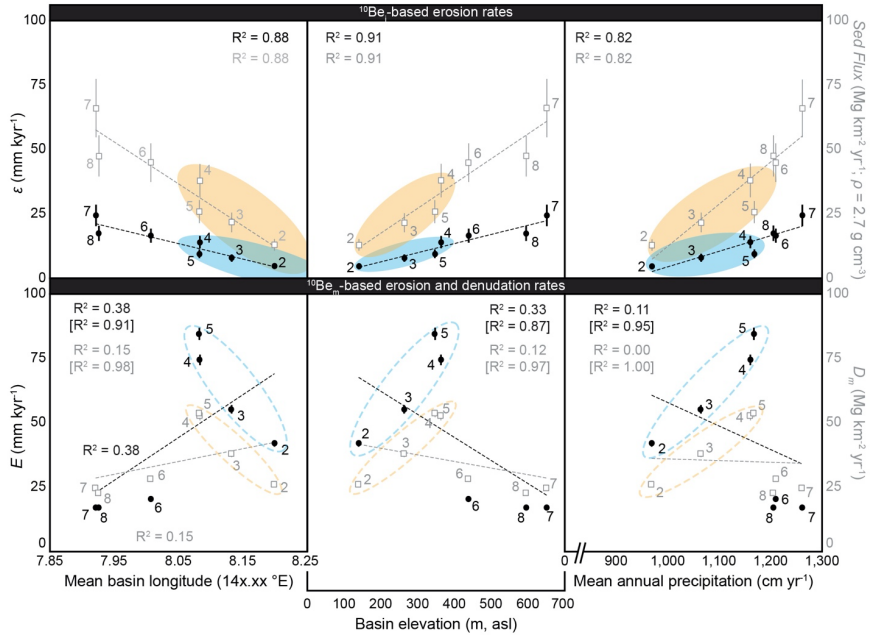

445 ~~**Figure 6: ^{10}Be, based erosion rates (ε, top row, black circles), ε-based sediment fluxes (top row, gray squares), ^{10}Be$_m$-based erosion rates (E, bottom row, black circles), and ^{10}Be$_m$/^{9}Be$_{reac}$-based denudation rates (D_m, bottom row, gray squares) from George River tributaries compared to mean basin longitude, mean basin elevation, and mean annual precipitation within each basin. ε for all tributaries and E and D_m for the central and eastern tributaries (orange and blue ellipses, respectively) are strongly correlated with each variable, likely owing to the East-West precipitation gradient projected across the catchment (Fig.**~~

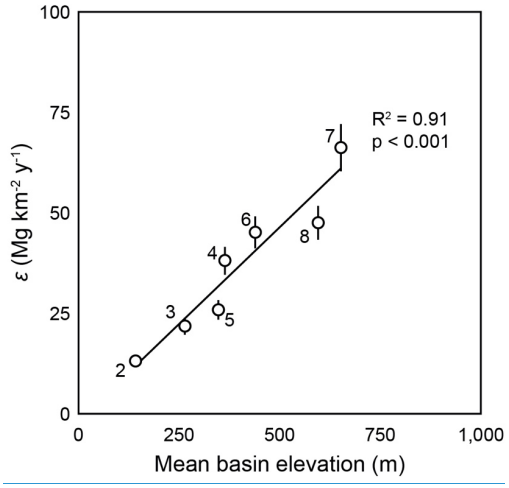

Figure 6: A strong correlation between $^{10}Be_i$ based erosion rates (ε) and mean basin elevation for the seven tributary samples collected in this study. We do not include data from trunk channel samples because they may incorporate sediment upstream of trunk channel sites but downstream of tributary sites (see Discussion).

4.2 $^{10}Be_m$ denudation rates, D_m

~~$^{10}Be_m$ 2). Unbracketed R^2 values reflect correlation of all data whereas bracketed R^2 values indicate correlations for $^{10}Be_m$-based metrics only in the central and eastern tributaries. All error bars show 2σ uncertainties.~~

Formatted: Font: 10 pt, Not Bold

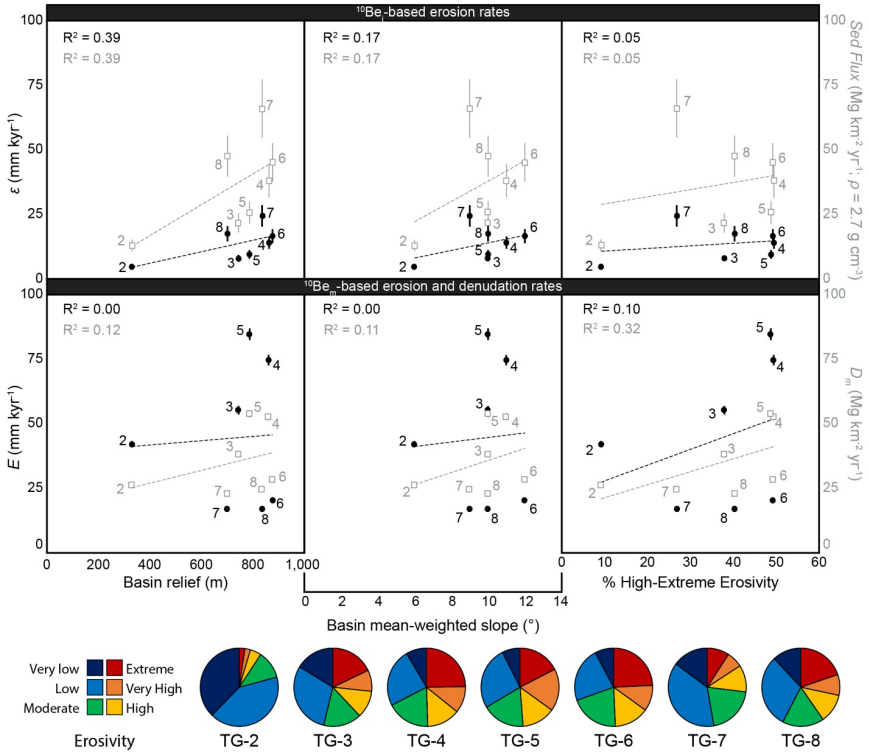

~~**Figure 7: ^{10}Be, based erosion rates (ε, top row, black circles), ε-based sediment fluxes (top row, gray squares), ^{10}Be$_m$-based erosion rates (E, bottom row, black circles), and ^{10}Be$_m$/^{9}Be$_{reac}$-based denudation rates (D_m, bottom row, gray squares) from George River tributaries compared to mean basin longitude, mean basin elevation, and mean annual precipitation within each basin. Moderate relationships exist between ε and basin relief and between D_m and the percent of each basin that is designated High Erosivity or greater (Kidd et al., 2014, 2015). All error bars show 2σ uncertainties.**~~

Formatted: Font: 10 pt, Not Bold

~~**4.2 ^{10}Be$_m$ erosion rates, E, and denudation rates, D_m**~~

~~^{10}Be$_m$ based erosion rates, E,~~ D_m, range from ~~17.0 to 78.3 mm kyr^{-1} and replicate values for ε well in the three westernmost headwater catchments, but not in the lower-elevation, center and easternmost tributaries, where E is systematically ~5–6x higher than ε (Fig. 8). ^{10}Be$_m$/^{9}Be$_{reac}$ based denudation rates, D_m, range from 22.7 to 53.7 Mg km^{-2} yr^{-1}. Except for TG-4 and TG-9, values for D_m~~ 27.4 to 60.5 Mg km^{-2} y^{-1}. Values for D_m in tributaries do not replicate ~~sediment fluxes~~ ^{10}Be$_i$-derived ~~from~~

Formatted: Font: Not Italic

~~ε, although the central and easternmost tributaries plot much closer to a 1:1 line than the samples from the three western-most headwater tributaries (Fig. 8). TG-4 was collected~~ erosion rates, ε, in any basin (Fig. 7). Neither does the $^{10}Be_m/^9Be_{reac}$-based denudation rate at the ~~mouth of Groom River, upstream of which activities at the long-closed Anchor Mine significantly altered the topography. The meteoric erosion rate for the~~ trunk channel site ~~TG-9, E = 78.3 ± 2.2 mm kyr^{-1} is significantly higher than ε for the same site (10.7 ± 1.7 mm kyr^{-1}), but the denudation~~, TG-9 (38.4 ± 0.5 Mg km^{-2} y^{-1}), replicate the $^{10}Be_i$ erosion rate ~~at TG-9, D_m = 33.0 ± 0~~(22.4 ± 1.9 Mg km^{-2} ~~yr^{-1}, replicates the ε-based sediment flux (28.9 ± 4.5 Mg km^{-2} yr~~y^{-1}).

In general, $^{10}Be_m$-based measures D_m of ~~E and D_m~~tributaries are not significantly related to any topographic or ~~climatic~~basin metric ~~(Figs. 6, 7). However, the observed relationships between E and D_m and longitude, elevation, and precipitation are similar to those observed~~such as mean basin elevation, mean local relief, or mean basin slope (R^2 = 0.12, R^2 = 0.06, R^2 = 0.11, respectively; $p > 0.44$). $^{10}Be_m$-based measures D_m of tributaries appear to be moderately related to the percentage of each basin that Kidd et al. (2014, 2015) categorizes with ~~ε in the central and eastern tributaries (Fig. 6); E and D_m in the western tributaries do~~ a land use of "High" to "Extreme" erosivity, though we note this relationship is not ~~follow the spatial trends that ε exhibits.~~significant (R^2 = 0.42; $p = 0.18$; Fig. 8).

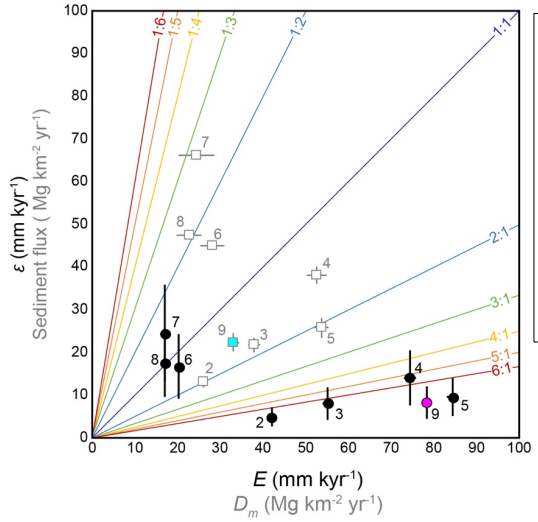

~~**Figure 8: $^{10}Be_i$-based erosion rates, ε, compared to $^{10}Be_m$-based erosion rates, E (black circles) and ε-derived sediment fluxes compared to $^{10}Be_m/^9Be_{reac}$-based denudation rates, D_m, (gray squares) for the same sample sites. Erosion rates for the trunk-channel sample, TG-9 are indicated by the magenta circle and denudation rates are indicated by the cyan square. All error bars show 2σ uncertainties. Solid colored lines indicate 1-fold through 6-fold differences between erosion and denudation metrics using the $^{10}Be_i$ and $^{10}Be_m$ methods. $^{10}Be_m$ erosion rates are ~5–6x greater than $^{10}Be_i$ erosion rates in the central and eastern tributaries. $^{10}Be_m/^9Be_{reac}$ denudation rates replicate $^{10}Be_i$ sediment fluxes with much greater accuracy than $^{10}Be_m$ erosion rates.**~~

Formatted: Left

Formatted: Font: Not Italic

4.3 Dissolved load and suspended sediment fluxes

The total dissolved sediment load in the George River at St. Helens for the 26 years between 1969 and 2020 is between 1,820 and 10,770 Mg y^{-1} (mean = 4,400 ± 2,230 Mg y^{-1}, 1σ) and the total suspended sediment load ranges from 280 to 10,560 Mg y^{-1} (mean = 1,830 ± 2,180 Mg y^{-1}, 1σ). The water treatment plant from which the dissolved load data were obtained is close to site TG-9, and data from this site allow us to place ^{10}Be-inferred erosion and denudation rates for the whole George River basin in context. These data show that the dissolved load export rate averages to about 10.3 Mg km^{-1} y^{-1}, which is <50% of ε (22.4 Mg km^{-2} y^{-1}), based on decades of flow records and five years of discontinuous water sampling at the same sampling location. The suspended sediment export rate out of the George River basin is less, 4.3 Mg km^{-2} y^{-1}.

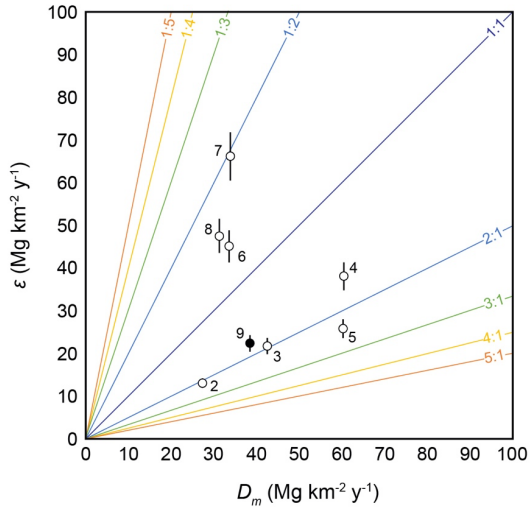

Figure 7: $^{10}Be_i$ based erosion rates (ε) compared $^{10}Be_m/^9Be_{reac}$-based denudation rates (D_m) for tributary basins (open circles) and the trunk channel site, TG-9 (closed circle). Measures of ε and D_m are different at each site, but similar within a factor of two.

5 Discussion

~~Erosion~~ The multi-methodological approach we employ in this study provides four new datasets, all of which quantify some component of landscape change at different spatial scales: (1) mass loss rates inferred $^{10}Be_i$ at seven tributary and two trunk channel sites, (2) denudation rates from $^{10}Be_m/^9Be_{reac}$ from seven tributary sites and one trunk channel site, (3) suspended sediment export at the mouth of the George River, and (4) the dissolved load of the George River from the water quality and flow data at the mouth of the catchment. Comparing and interpreting these new datasets improves our understanding of the rate of landscape change over time in the George River basin. Given that the only location for which we have data from all four of datasets is at the mouth of the George River in St. Helens, we explore what the different rates presented in this study

Formatted: Left

might mean for landscape change across the whole river basin, recognizing that without more data, we cannot be more specific in our interpretation of ε or D_m at tributary sites beyond traditional meanings of erosion or denudation, respectively.

5.1 Relationships between ε, elevation-dependent climate conditions, and land use

Erosion rates in the George River basin are strongly related to basin ~~longitude,~~ elevation, ~~and mean annual precipitation~~which varies greatly across the catchment as the study area extends east ~~of~~from the Rattler Range and ~~the prominent Ben Lomond Plateau~~Mt. Victoria (1,213 m) to the coast at sea-level (Fig. ~~6), and~~2). In contrast, we find no evidence to suggest that ε is related to slope in the George River over millennial timescales. This result differs from ~~most~~many studies, which show strong correlations between ε and mean basin slope at a global scale (Portenga and Bierman, 2011~~),~~) and at regional scales~~,~~ across the Great Dividing Range on Australia's mainland (Fig. 9; Codilean et al., 2021; Nichols et al., 2014~~), and despite~~). Our results also differ from prior assessments of the George River basin using measured climate data, bedrock structure, topographic analysis, water quality models, and geographical landscape characterization that suggest slope imparts a large control over erosion and sediment generation in the catchment on human timescales (Jerie et al., 2003; Kragt and Newham, 2009). ~~Instead, our finding is consistent with Mishra et al.'s (2018) suggestion that in low-slope, low-elevation, post-tectonic settings, the relationship between slope and erosion becomes secondary to precipitation, and this study presents one of the clearest examples of erosion along a topographically-induced precipitation gradient in ^{10}Be, erosion literature.~~

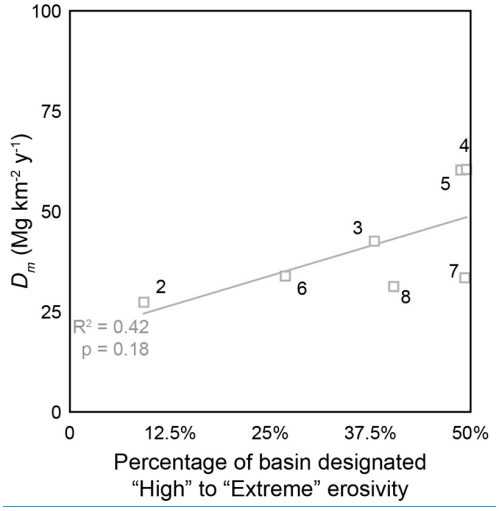

Figure 8: $^{10}Be_m/^9Be_{reac}$-based denudation rates, D_m, (gray squares) from tributary basins measured at George River are related to the percentage of the basin that is classified as "High," "Very High," or "Extreme" Erosivity (Kidd et al., 2014, 2015), though this relationship is not significant (p = 0.18). The basins with the highest denudation rates are those with histories of intensive mining and/or recent forestry, both of which disturb topsoils.

Formatted: Left

Any process-based explanation for the correlation of erosion rates with elevation requires that we consider how relevant geomorphic and geochemical processes vary across the George River basin. Climatic data collected from stations in and near the George River basin indicate that both mean annual temperature and mean annual precipitation are strongly correlated with elevation (Fig. 3).

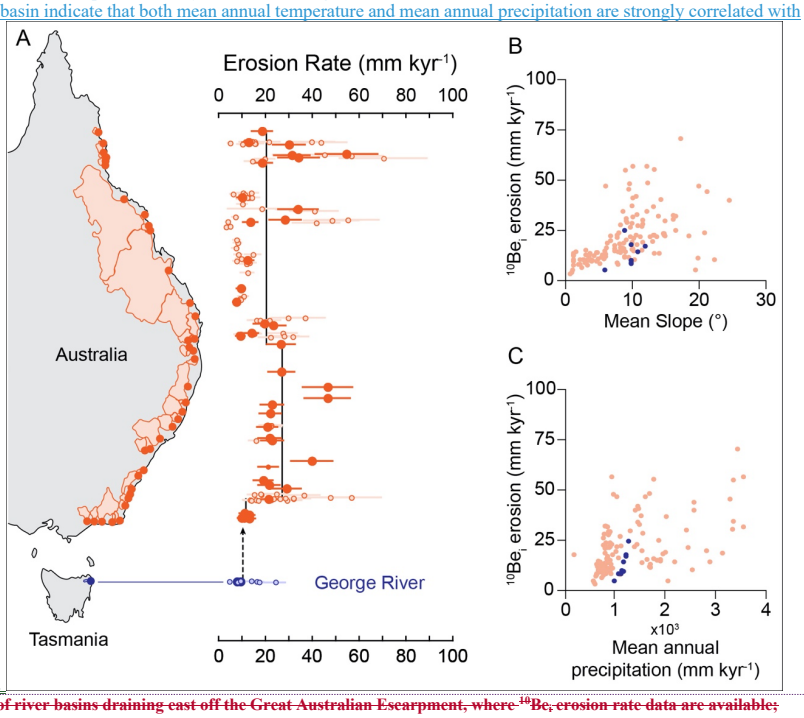

~~**Figure 9: A. Map of river basins draining east off the Great Australian Escarpment, where ^{10}Be, erosion rate data are available; adapted from Codilean et al. (**~~At higher elevations, rocks are experiencing lower temperatures more frequently and receive more precipitation than lower elevations, increasing the potential for both mechanical (frost cracking) and chemical weathering (dissolution). Frost cracking rates are greatest in rocks where mean annual temperature is above freezing (which is the case for all of the George River basin) but temperatures go below freezing both long and frequently enough to crack rocks, which is also the case across much of the basin (Delunel et al., 2010; Hales and Roering, 2007). In the George River basin, the only temperature-related metric that correlates with elevation is mean annual temperature, in contrast to, for example, the time spent below freezing, likely because temperature inversions, with cold air drainage to lower elevation valleys, are common (Webb et al., 2018, 2020). Additionally, the underlying mechanics that lead to rock fracturing in the first place have been demonstrated to be strongly linked to climate and the availability of water (Eppes and Keanini, 2017;

Formatted: Font: 10 pt, Not Bold

Eppes et al., 2018). While water is plentiful across the George River basin, we see that ε is greater at higher elevations where rainfall is also greater, facilitating faster breakdown of rock.

Mean annual precipitation at meteorology stations in the George River basin varies less (2.7-fold) from low to high elevations (681–1,836 mm y^{-1}; Fig. 3) than ε (4.8–24.5 mm ky^{-1}; a 5.1-fold difference; Table 4). The elevation-induced precipitation and erosion rate gradients we observe are consistent with suggestions made at regional and global scales that the relationship between slope and erosion becomes secondary to precipitation in low-slope, low-elevation, post-tectonic settings (Henck et al., 2011; Mishra et al., 2018). We note that Mishra et al. (2018) also suggest that at the global scale, the erosional effects of increased of precipitation may be balanced by increased vegetation cover, which serves to stymy erosion. However, the George River basin is densely vegetated throughout, and forests are no more prevalent at higher than lower elevations in our field area. We propose that in the George River basin, ε is related to elevation in large part because precipitation is strongly correlated with elevation. This interpretation seems to hold true for bedrock outcrops, the erosion rates of which are most-closely correlated to mean annual rainfall in aseismic landscapes; however, basin-wide erosion rates in aseismic areas globally remain more strongly correlated to mean basin slope and subsequently to elevation and climate-related processes (Portenga and Bierman, 2011), which stands in contrast to the relationship we observe here between elevation and ε.

~~2021). Filled circles are trunk streams and open circles are tributaries. Orange data include previously published data (Codilean et al., 2021; Croke et al., 2015; Fülöp et al., 2020; Godard et al., 2019; Nichols et al., 2014; Tomkins et al., 2007). Blue data are new data presented in this study from George River, Tasmania. The average $^{10}Be_i$ erosion rates from George River (10.5 mm kyr^{-1}) is consistent with erosion rates from southeast mainland Australia (average 11.6 mm kyr^{-1}; Codilean et al., 2021). B. Comparison of $^{10}Be_i$ erosion rates from George River (blue circles) and the eastern flanks of the Great Australian Escarpment (orange circles) to basin average slope. B. Comparison of $^{10}Be_i$ erosion rates from George River (blue circles) and the eastern flanks of the Great Australian Escarpment (orange circles) to mean annual precipitation.~~

Formatted: Font: 10 pt, Not Bold

The very strong relationship between ~~precipitation~~elevation, climate (both mean annual rainfall and temperature), and ε would likely not have emerged had our $^{10}Be_i$ samples been affected by clast attrition (Carretier et al., 2009), deep-seated landslides (Aguilar et al., 2014; Gonzalez et al., 2016; Puchol et al., 2014), or intensive erosion associated with mining, forestry, or agriculture (Barreto et al., 2014; Neilson et al., 2017). Even intensive tin mining, which supplied >10^6 m^3 to the George River over the last two centuries (Knighton, 1991) seems ~~to~~ not to have ~~not~~ had a long-lasting diluting effect on $^{10}Be_i$ in sampled stream sediment. It is possible that mining efforts, especially ~~the~~ sluice mining, did not lead to $^{10}Be_i$ dilution because of the homogenizing effect of $^{10}Be_i$ in ~~well~~ bioturbated soils (Brown et al., 1995) or ~~that~~because the size of the George River ~~was~~basin is large enough to buffer the effects of mining efforts in a similar way that large catchments ~~can~~may buffer the effects of landslide material (Niemi et al., 2005; Yanites et al., 2009). It is also possible that mining activity did lead to $^{10}Be_i$ dilution, but ~~that these effects~~concentrations have ~~since recovered~~normalized along with bedload characteristics

(Knighton, 1991)), similar to the rapid, two-year recovery of $^{10}Be_i$ concentrations following storm-triggered landslides in Puerto Rico (Grande et al., 2021).

Overall, the close relationship between $^{10}Be_i$ erosion rates and mean annual precipitationclimate across the George River basin demonstrates how wellthat $^{10}Be_i$ erosion rates can reflect background, geologically-meaningful rates of landscape evolution on millennial timescales, even in areas with long histories of intensive human land-use. (e.g. Barreto et al., 2014; Rosenkranz et al., 2018; Vanacker et al., 2007). Secondarily, that higher values of ε are observed where there is more rainfall and are colder temperatures suggests that more sediment is being generated in the western portion of the catchment. There, larger volumes of rainfall and colder temperatures facilitate the generation, erosion, entrainment, and delivery of more sediment to trunk channels than in the eastern portion of the catchment.

Higher values of ε where there is more rainfall suggests that more sediment is being generated in the western portion of the catchment where larger volumes of rainfall can facilitate the generation, erosion, entrainment, and delivery of sediment to trunk channels than in the eastern portion of the catchment. However, we recognize that perhaps ε is not necessarily related to precipitation, but rather ε and precipitation may both be more directly influenced by elevation. Although no part of George River was ever glaciated, cirque development and periglacial activity was active to the southwest of George River, across the Ben Lomond Plateau during the Last Glacial Maximum and previous glaciations (Barrows et al., 2002; Colhoun, 2002), in which case ε may be greater at higher elevations due to greater amounts of periglacial weathering.

High $^{10}Be_i$ erosion rates have been linked to greater amounts of periglacial activity elsewhere (e.g. Delunel et al., 2010; Hancock and Kirwan, 2007; Marshall et al., 2017); however, periglacial activity in northeast Tasmania was typically limited to elevations >1,100 m (Colhoun, 2002), and it is therefore unlikely that periglacial processes would have increased erosion rates in George River's western tributaries, all of which are below this elevation. Alternatively, higher ε at higher elevations may be due to greater amounts of rock exhumation for inland northeast Tasmania relative to the coasts throughout the Cenozoic, interpolated from apatite fission track cooling ages across Tasmania (Kohn et al., 2002). This is also unlikely, however, as landscape lowering over millions of years has slowed from an early Cenozoic peak rates of 30–50 m Myr^{-1} to late Cenozoic rates of <10 m Myr^{-1}, and rock exhumation rates are presently comparable, if not slower than new $^{10}Be_i$ based erosion rates presented in this study. We therefore remain confident that the relationship between ε and elevation and rainfall in this study are real and reflective of the influence of rainfall in driving landscape evolution over millennial timescales in George River.

Since pre-disturbance stream flow and bedload conditions were re-established by the 1990s (Knighton, 1991), it appears the greatest risk of future excesses ofenhanced sediment flux from the George River to Georges Bay in the future comes from land-use changes involving the widespread disturbance of surficial soils, such as through forestry (Wilson, 1999). The

Formatted: Left, Border: Top: (No border), Bottom: (No border), Left: (No border), Right: (No border), Between : (No border)

Formatted: Left

Formatted: Left

percentage of land used for ~~Production~~production forestry in native environments has been decreasing throughout the 21st century (Fig. 4), and while some of this land use is being supplanted by Conservation and Protected Native Land Cover, which could buffer the effects of widespread erosion, much is being replaced by grazing and agriculture, which would ~~only serve to~~likely increase erosion, particularly in the headwater catchments where geological erosion rates are naturally ~~high~~higher (Fig. 4). Given recent land-use trends, the $^{10}Be_i$ erosion rates presented here ~~may~~ provide a useful benchmark level of sediment delivery to the George River, Georges Bay, and other fluvial systems in northeast Tasmania that share topographic and geologic characteristics similar to those ~~at~~of the George River basin.

5.~~1~~2 Considerations of ε for trunk channel versus tributary sites

~~A~~The mass ~~balance comparison of the volume of sediment~~ leaving the tributaries (10,511 ± 394 Mg y^{-1}) is about the same as the mass passing through ~~the trunk channels (ε x upstream area; 3.8 ± 0.7 km^3 yr^{-1} at~~ TG-1 (10,286 ± 859 Mg y^{-1}) and ~~3.5 ± 0.7 km^3 yr^{-1} at TG-9) versus the summed volume of sediment exiting tributaries (3.9 ± 0.3 km^3 yr^{-1}) suggests that little erosion (and therefore addition of sediment) is occurring in the trunk channel subcatchments. Average modelled ε for trunk channel sites, calculated using the regression equations and mean longitude, the mean elevation, and mean annual precipitation values for the TG-1 and TG-9 subcatchments (9.6 ± 3.0 mm kyr^{-1} and 1.1 ± 3.1 mm kyr^{-1}, respectively), however, suggests that the TG-1 subcatchment should be contributing at least ~1 km^3 of sediment more to George River annually. Given that the mass of sediment leaving the tributaries is equal to the~~ the mass of sediment ~~passing through TG-1 and TG-9, we make the interpretation~~leaving TG-9 (9,555 ± 817 Mg y^{-1}). We infer from these data that the $^{10}Be_i$ measured at TG-1 and TG-9 trunk channel locations is ~~effectively~~ dominated by ~~erosion~~mass loss in the ~~tributaries.~~higher-elevation tributary basins with ~~little~~minimal sediment input from the ~~subcatchments or George River floodplain, and ε at trunk channel sites should be considered minimum estimates of erosion for the upstream contributing area. Our interpretation of erosion at trunk streams being dominated by headwater input has~~George River valley bottoms. Similar interpretations have been made elsewhere, albeit in much larger river basins (i.e.~~.~~, Wittmann et al. 2009, 2011, 2016). ~~The~~ Given these similarities, we average ε from the two trunk channel sites to produce a nominal average erosion rate ~~we therefore present for George River is the average of ε at TG-1, TG-9, and the average of ε from the seven tributaries combined (10.5 ± 0.8 mm kyr^{-1}); we do not consider ε of trunk channel samples, modelled or measured, when considering spatial statistics of erosion in~~ for the George River basin~~.~~

~~Compared to measurements of ε on the Australian mainland, the mean value of ε for George River (10.5 ± 0.8 mm kyr^{-1})~~ as a whole (24.1 ± 1.4 Mg km^{-2} y^{-1}; or 8.9 ± 0.5 mm $ky^{-1}$when dividing ε by rock density, ρ = 2.7 g cm^{-3}), which is of similar magnitude ~~as~~to the ~~median~~average erosion rate ~~for all~~of catchments draining the eastern flanks of the Great Dividing Range along the southeastern passive margin of mainland Australia (~~15.9~~11.6 mm ~~kyr~~ky^{-1}; Fig. 9; Codilean et al., 2021). Average ε from the George River basin is most consistent~~, however,~~ with ~~the~~ erosion ~~rates~~ of ~~mainland~~ basins ~~at the southernmost extent of the Great Dividing Range,~~ across the Bass Strait, which ~~are those that~~ share similar topographic characteristics and geological histories as the George River basin (Codilean et al., 2021). The similarity between the geology, topography, and

Formatted: Font: Not Italic

Formatted: Left, Border: Top: (No border), Bottom: (No border), Left: (No border), Right: (No border), Between : (No border)

Formatted: Left

Formatted: Left

climate~~, and topography~~ of newly-sampled basins and derived $^{10}Be_i$ erosion rates in Tasmania from this study and those from southeast mainland Australia ~~suggests~~supports the notion that evolution of landscapes that share similar climatic, topographic, and geologic characteristics is ~~driven by common forces.~~similar.

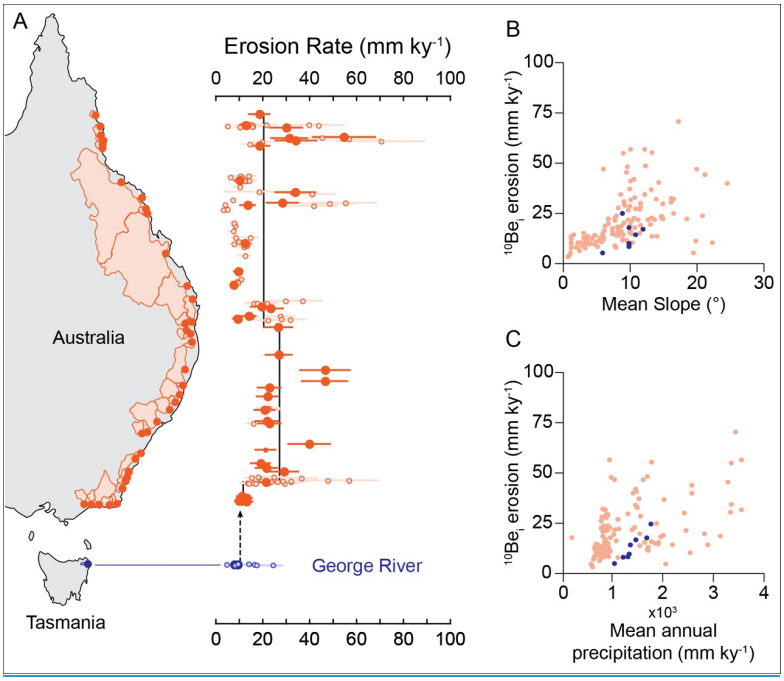

Figure 9: A. Map of river basins draining east off the Great Australian Escarpment, where $^{10}Be_i$ erosion rate data are available; adapted from Codilean et al. (2021). Filled circles are trunk streams and open circles are tributaries. Orange data include previously-published data (Codilean et al., 2021; Croke et al., 2015; Fülöp et al., 2020; Godard et al., 2019; Nichols et al., 2014; Tomkins et al., 2007). Blue data are new data presented in this study from the George River basin, Tasmania. The average $^{10}Be_i$ erosion rates from the George River (8.9 mm ky^{-1}) is consistent with erosion rates from southeast mainland Australia (average 11.6 mm ky^{-1}; Codilean et al., 2021). B. Comparison of $^{10}Be_i$ erosion rates from the George River basin (blue circles) and the eastern flanks of the Great Australian Escarpment (orange circles) to basin average slope. C. Comparison of $^{10}Be_i$ erosion rates from the George River basin (blue circles) and the eastern flanks of the Great Australian Escarpment (orange circles) to mean annual precipitation; in this comparison, mean annual precipitation for George River samples comes from the elevation scaling for measured rainfall at meteorological gauging stations (Figs. 2, 3, Table 1) whereas Codilean et al. (2021) summarize precipitation data for mainland basins from the WorldClim database (Fick and Hijamans, 2017).

Formatted: Left, Border: Top: (No border), Bottom: (No border), Left: (No border), Right: (No border), Between : (No border)

5.~~2~~3 Comparing $^{10}Be_i$-based erosion rates and $^{10}Be_m$-based ~~erosion and~~ denudation ~~metrics~~rates

~~The~~Once delivered to Earth's surface in temperate regions, $^{10}Be_m$ concentrates in uppermost soil horizons (Graly et al., 2010; Willenbring and von Blanckenburg, 2010). This behaviour differs from that of $^{10}Be_i$, the concentration of which remains homogenous in well-mixed, bioturbated soils for millennia (Jungers et al., 2009). Thus, any disturbance of large volumes of topsoil (i.e., agriculture, forestry, wildfire erosion, or mining activities) strips material with the highest concentrations of $^{10}Be_m$ and introduces that material into streams, a process similar to that identified following early land-use changes and deforestation in the Chesapeake Bay and San Francisco Bay (Portenga et al., 2019; Valette-Silver et al., 1986; van Geen et al., 1999). In contrast, the strong relationship between $^{10}Be_i$ erosion rates and ~~topographically-induced~~elevation, and thus both precipitation and temperature, across ~~Georges~~the George River basin (Fig. 6) suggests that $^{10}Be_i$ erosion rates, ε, are ~~geologically accurate and meaningful. The small, geologically-homogeneous landscape of George River, therefore allows us to test a previous hypothesis (Portenga et al., 2019) that measured $^{10}Be_m$-based erosion rates, E, and $^{10}Be_m/^{9}Be_{reac}$-based denudation rates, D_m, to~~ unaffected by land use.

Calculated values of D_m do not replicate ε~~, or ε-based sediment fluxes, respectively. At first glance, E replicates ε only in the headwater catchments and D_m replicates ε-based sediment fluxes relatively well in all tributaries except for the headwater catchments~~ (Fig. ~~8). Overall, values of E and D_m do not~~7), nor does D_m replicate the spatial patterns or yield the same relationships with topographic and climate parameters that we observe with ε ~~and ε-based sediment fluxes (Figs. 6, 7). However, when only E and D_m from tributaries in the central and eastern areas of George River (TG-2 through TG-5) are considered, a consistent relationship between E and D_m and basin longitude, elevation, and precipitation emerges and is similar to the relationships we observe between longitude, elevation, and precipitation and ε (Fig. 6). Despite this small sample subset (n = 4), we suggest that E and D_m reflect the same patterns of landscape dynamics in George River as ε. Moreover, the~~ in the small, geologically-homogeneous landscape of the George River basin (e.g., Fig. 6). We know that decades-old historical mining activities and historical bushfires in the George River were restricted to lower catchment areas and tributaries where measurements of D_m are highest (Figs. 4, 8). Additionally, we infer from the moderate correlation observed between D_m and the percent of tributary basins classified as "High" to "Extreme" Erosivity (R^2 = 0.33; Fig. 8; Kidd et al., 2014, 2015) that $^{10}Be_m/^{9}Be_{reac}$-derived denudation rates appear to be sensitive to recent land-use practices that disturb soils. The highest denudation rates, D_m, we measured are those from basins with past histories of intense surface disruption through mining and forestry (i.e., TG-4, TG-5).

The similarity of D_m and ~~ε-based sediment fluxes for central and eastern tributaries~~ for the entire George River basin, ~~however—within a factor of 2 (Fig. 7)—~~provides general support ~~our~~for the hypothesis that $^{10}Be_m/^{9}Be_{reac}$-based denudation rates ~~should~~ more-closely ~~replicate~~resemble $^{10}Be_i$-based erosion rates in small river basins where geological heterogeneity is minimized. ~~Our findings also, generally, support~~This observed similarity between D_m and ε supports the continued exploration and application of $^{10}Be_m/^{9}Be_{reac}$ denudation rates in geomorphological studies. However, data presented here

Formatted: Left

Formatted: Font: Italic

suggest that this method should be used with caution in landscapes with recent soil disturbance (Dannhaus et al., 2017; Deng et al., 2020; Portenga et al., 2019; Rahaman et al., 2017; Wittmann et al., 2012, 2015). ~~Interestingly, measured values of *E* are systematically ~4–5x greater than *ε*, and thus while *E* may be influenced by the same geomorphological processes in~~

5.4 Where does the dissolved load originate in the George River basin?

If chemical weathering occurs primarily in the uppermost meters of the landscape, where most $^{10}Be_i$ is produced, then the erosion rate, ε, we calculate represents landscape mass loss over time—a combination of physical and chemical mass loss. We could then partition ε along the trunk channel at the mouth of the George River basin (TG-9 = 22.4 Mg km^{-2} y^{-1}) into mass flux removed in dissolved load (10.3 Mg km^{-2} y^{-1}) and the remainder, mass flux removed as solid sediment (12.1 Mg km^{-2} y^{-1}). Of the sediment mass flux, it appears that 4.3 Mg km^{-2} y^{-1} is transported as suspended load and 7.8 Mg km^{-2} y^{-1} is bedload. Our measure of ε at TG-9 is ~40% lower than the $^{10}Be_m/^{9}Be_{reac}$ measure of denudation at this site (38.4 Mg km^{-2} y^{-1}), which if the assumptions of the method are met, represents total physical and chemical mass loss. Taken at face value, either D_m overestimates total mass loss from the George basin at TG-9 or ε underestimates denudation, both by 40%. Coincidentally, an independent measure of weathering at TG-9, based on $^{9}Be_{min}$ and $^{9}Be_{reac}$ data (equation 9 in Wittmann et al., 2015) suggests that there is a ~40% weathering degree at this site, which suggests that ε underestimates denudation.

If the majority of chemical weathering occurs below the penetration depth of most cosmic rays (< 2 m), then the chemical denudation and physical mass loss are at least in part and perhaps wholly disconnected. In this case, ε (TG-9 = 22.4 Mg km^{-2} y^{-1}) would need to be summed with the chemical mass flux (10.3 Mg km^{-2} y^{-1}) and together (30.7 Mg km^{-2} y^{-1}), they would estimate the total mass loss from the landscape. The presence of bedrock outcrops in some of the George River basin channels suggests that regolith thickness is limited in places and in that case, $^{10}Be_i$ measurements incorporate much of the chemical mass loss from the basin. However, the few boreholes that extend to unweathered bedrock (n = 3; Fig. 2; Table 1) clearly indicate that regolith is deeper in some parts of the catchment. With the paucity of available data, we cannot determine how much of the dissolved load is coming from below the penetration depth of cosmic-ray neutrons but it could be significant.

Summing ε and the dissolved load (30.7 Mg km^{-2} y^{-1}) results in a total mass loss more consistent with that suggested by $^{10}Be_{met}/^{9}Be_{reac}$-based denudation rate at TG-9, D_m = 38.4 Mg km^{-2} y^{-1}. Yet, the $^{10}Be_{met}/^{9}Be_{reac}$-based denudation rates appear to have little correlation with landscape scale metrics—and are highest in basins with known histories of intensive land-use disturbance and erosivity (Figs. 2, 8)—making it uncertain they still reflect the rate of geomorphic processes controlling mass loss over time. In contrast, ε is well-correlated to elevation and thus temperature and precipitation. With the data set presented here, it is not yet possible to know if the balance between physical and chemical mass loss in tributaries is consistent with what we observe at the mouth of George River ~~as *ε* and D_m, it does not appear to reflect accurate rates of landscape change~~.

Formatted: Left, Border: Top: (No border), Bottom: (No border), Left: (No border), Right: (No border), Between : (No border)

~~The similarity of the spatial patterns of E and D_m with longitude, elevation, and precipitation in the central and eastern tributaries with those exhibited by ϵ across the whole George River basin suggests that E and D_m in the headwater catchments (TG-6, TG-7, and TG-8) significantly underestimate accurate or realistic values of E and D_m for these tributaries. Of all of the variables and measurements required to derive both E and D_m, excess amounts of measured $^{10}Be_m$ is the only common factor that would lead to erroneously low calculated values of E and D_m. Once delivered to Earth's surface, meteoric $^{10}Be_m$ concentrates in uppermost soil horizons (Graly et al., 2010; Willenbring and von Blanckenburg, 2010), and thus any disturbance and excavation of large volumes of topsoil (i.e. agriculture, forestry, wildfire erosion, or mining activities) could strip soil with the highest concentrations of $^{10}Be_m$ in its grain coatings entering and introduce them into a stream's bedload, a process similar to that identified following early land-use changes and deforestation in the Chesapeake Bay and San Francisco Bay (Valette-Silver et al., 1986; van Geen et al., 1999). Mining activities in George River were restricted to lower catchment areas and tributaries where $^{10}Be_m$ based metrics demonstrate the same relationships to topography and climate as ϵ (Fig. 2), and no wildfires nor prescribed fires have burned through the headwater catchments (Fig. 4).~~

~~At the time of sample collection for this study in 2008, forestry from natural environments and from production plantations was the largest land use designation within George River. Elsewhere in George River, rainfall and runoff experiments carried out in the Gentle Annie experimental catchment, a tributary to TG-2 (Fig. 4), showed that rills and gullies developed in hillslope plots that were heavily disturbed by forestry machinery, yielding significantly more sediment during simulated rainfall events than soil plots that were burned and more sediment than plots where soils were left undisturbed (Wilson, 1999). Although there are no detailed records of when plots of land in George River were timbered, we invoke Wilson's (1999) findings to suggest it is plausible that active forestry had disturbed soils in the headwater catchments at or shortly prior to the timing of sample collection, significantly disturbing $^{10}Be_m$-rich top soils, and delivering large volumes of sediment with excess $^{10}Be_m$ to sample collection sites, which subsequently resulted in the calculated values of E and D_m that are much lower than otherwise expected based on the trends of E and D_m in other tributaries. Following this interpretation, we suggest that measures of E and D_m may reflect spatial patterns or replicate ϵ rates in geologically homogeneous landscapes, respectively, but caution should be taken when applying $^{10}Be_m$ erosion and denudation metrics in landscapes with intensive soil disturbances (Portenga et al., 2019).~~

6 Conclusions

The $^{10}Be_i$-based erosion rates ~~throughout the George River basin, and $^{10}Be_m$ erosion and denudation rates~~we present in ~~its central and eastern tributaries,~~this study are ~~closely related~~the first derived for any river system for Tasmania. In contrast to ~~a topographically-induced East-West precipitation gradient~~ erosion across the ~~catchment. Tasmanian landscapes differ from the~~ Great Dividing Range on mainland Australia where erosion rates and mean basin slope are closely linked~~.~~, erosion in the George River basin has a strong relationship with mean basin elevation, and thus with mean annual precipitation and mean

Formatted: Font: Bold

Formatted: Left, Border: Top: (No border), Bottom: (No border), Left: (No border), Right: (No border), Between : (No border)

Formatted: Left

Formatted: Font color: Black

annual temperature, which are both strongly correlated with elevation. The average $^{10}Be_i$ erosion rate in the George River~~, 13.6 mm kyr~~ basin, 24.1 ± 1.4 Mg km^{-2} y^{-1}, reflects erosion in tributaries to the George River where precipitation is greatest and temperatures are lowest; little sediment is generated in trunk channel ~~subcatchments.~~valley bottoms. These findings support the notion that precipitation imparts ~~more~~a significant influence on landscape development in low-slope, low-elevation landscapes ~~(Mishra et al., 2018).~~, which are often ~~tend to be~~located in post-orogenic, passive margin settings.

We also suspect that low but positive mean annual temperatures with frequent excursions below zero drives the mechanical breakdown of rock, thereby increasing sediment production in high-elevation basins through frost cracking. Although ~~sediment~~hillslope erosion associated with mining, agricultural, and forestry land-use practices occurred in the George River basin during the 19th and 20th ~~Centuries~~centuries, $^{10}Be_i$ based erosion rates in the basin appear to reflect pre-disturbance rates of landscape change. Such rates are useful as part of Tasmania's current efforts to re-establish healthy and sustainable ecological conditions in its many estuarine environments, particularly those in northeast Tasmania where estuary tributaries have similar geological and topographic characteristics to those found ~~at George River. The pace of erosion in the George River basin is similar to that at the southern end of the Great Dividing Range on the Australian mainland, which has similar bedrock and climate characteristics.~~ in the George River basin. $^{10}Be_m/^9Be_{reac}$ denudation rates in the central and eastern tributaries of the George River basin generally replicate $^{10}Be_i$-based erosion within a factor of two, but they do not replicate $^{10}Be_i$ erosion data at any sample site, likely owing to intensive topsoil disturbance during decades and centuries of mining, forestry, and agricultural land use. Data from the George River basin support application of $^{10}Be_m/^9Be_{reac}$ denudation rates in small, lithologically homogeneous basins with limited amounts of topsoil disturbance.

~~$^{10}Be_m$ based erosion and denudation in the central and eastern tributaries of George River generally replicates spatial patterns of $^{10}Be_i$ based erosion and denudation. Low $^{10}Be_m$ based erosion and denudation rates calculated in three headwater tributaries demonstrate the sensitivity of meteoric ^{10}Be based calculation to recent and intensive land use that disturbs and erodes topsoils. Data from the George River basin support application of $^{10}Be_m$ methods in small, lithologically homogeneous basins with limited amounts of topsoil disturbance.~~

~~**Appendices**~~

Formatted: Font color: Auto, Not Highlight

Formatted: Left

Formatted: Not Superscript/ Subscript

Appendix A: Erosion rate and denudation rate equations

$^{10}Be_i$ *Erosion Rate*

$$\varepsilon = \frac{\Lambda\left(\frac{P_0}{N} - \lambda\right)}{\rho}$$

$^{10}Be_i$ *Sediment Flux*

$$Sed\ Flux = \varepsilon\,\rho$$

$^{10}Be_i$ *Integration Time*

$$Int\ Time = \frac{\Lambda\,\varepsilon}{\rho}$$

$^{10}Be_m$ *Erosion Rate*[d]

$$E = \frac{Q}{\rho\ {}^{10}Be_m}$$

$^{10}Be_m/^{9}Be_{reac}$ *Denudation Rate*[e]

$$D_m = \frac{Q\left(\frac{{}^{9}Be_{min}}{{}^{9}Be_{reac}} + 1\right)}{\left(\frac{{}^{10}Be_m}{{}^{9}Be_{reac}}\right){}^{9}Be_{parent}}$$

Variable	Description	Unit
ϵ	$^{10}Be_i$ erosion rate	cm yr^{-1}
Λ	Attenuation length for cosmic-ray penetration[a]	160 g cm^{-2}
P_0	Production rate of $^{10}Be_i$ at Earth's surface[b]	atoms g^{-1} yr^{-1}
N	Measured concentration of *in-situ* produced $^{10}Be_i$	atoms g^{-1}
λ	^{10}Be decay constant[c]	yr^{-1}
ρ	Rock density	2.7 g cm^{-3}
E	$^{10}Be_m$-based erosion rate	cm yr^{-1}
Q	Atmospheric $^{10}Be_m$ delivery rate	atoms cm^{-2} yr^{-1}
$^{10}Be_m$	Measured concentration of $^{10}Be_m$ extracted from sediment grain coatings	atoms g^{-1}
D_m	$^{10}Be_m/^{9}Be_{reac}$-based denudation rate	g cm^{-2} yr^{-1}
$^{9}Be_{min}$	Measured concentration of ^{9}Be still within mineral grains	atoms g^{-1}
$^{9}Be_{reac}$	Measured concentration of ^{9}Be extracted from sediment grain coatings	atoms g^{-1}
$^{9}Be_{parent}$	Assumed concentration of ^{9}Be in crustal bedrock[f]	1.671 x 10^{17} atoms g^{-1}

[a] Balco et al. (2008), Gosse and Phillips (2001)
[b] Scaled for each basin following Lal (1991) and Stone (2000)
[c] Half-life of ^{10}Be = 1.36 Myr
[d] Willenbring and von Blanckenburg (2010)
[e] von Blanckenburg et al. (2012)
[f] Derived from an assumed value of 2.55 ppm, following von Blanckenburg et al. (2012)

Appendix B: CRONUS Entry Data

TG-1	-41.29017	148.22217	346	std	1	2.7	0	2008	;
TG-1	Be-10	Quartz	3.64E+05	6.52E+03	07KNSTD	;			
TG-2	-41.27183	148.19925	141	std	1	2.7	0	2008	;
TG-2	Be-10	Quartz	5.66E+05	7.72E+03	07KNSTD	;			
TG-3	-41.28286	148.13247	265	std	1	2.7	0	2008	;
TG-3	Be-10	Quartz	3.97E+05	1.17E+04	07KNSTD	;			
TG-4	-41.25514	148.08317	364	std	1	2.7	0	2008	;
TG-4	Be-10	Quartz	2.56E+05	6.95E+03	07KNSTD	;			
TG-5	-41.25364	148.08239	347	std	1	2.7	0	2008	;
TG-5	Be-10	Quartz	3.63E+05	8.48E+03	07KNSTD	;			
TG-6	-41.28067	148.00697	439	std	1	2.7	0	2008	;
TG-6	Be-10	Quartz	2.33E+05	5.05E+03	07KNSTD	;			
TG-7	-41.32208	147.92172	652	std	1	2.7	0	2008	;
TG-7	Be-10	Quartz	1.88E+05	5.60E+03	07KNSTD	;			
TG-8	-41.32178	147.92592	596	std	1	2.7	0	2008	;
TG-8	Be-10	Quartz	2.48E+05	6.10E+03	07KNSTD	;			
TG-9	-41.31350	148.26531	331	std	1	2.7	0	2008	;
TG-9	Be-10	Quartz	4.11E+05	9.92E+03	07KNSTD	;			

We would like to acknowledge the Palawa peoples of lutruwita, the traditional custodians of the lands on which this work was completed.

Formatted: Left

Data Availability

All maps were created by EWP; data within maps (e.g. DEMs, geology, etc.) is properly cited. All data used in this study~~,~~ and all data needed to reproduce our findings ~~are presented in Tables 1-3~~ and the equations ~~we use to work with data~~used to calculate $^{10}Be_i$ erosion rates~~, sediment fluxes,~~ and $^{10}Be_m/^{9}Be_{reac}$ denudation rates~~, and integration times~~ are presented in ~~Appendix A. Data entry for calculating erosion rates~~Tables 1–6. Mean annual precipitation and geological borehole data were gathered from ~~the CRONUS~~ online ~~erosion rate calculator, formatted for text entry, are given in Appendix.~~databases supported by the Australian Bureau of Meteorology (Rainfall: http://www.bom.gov.au/climate/data/; borehole: http://www.bom.gov.au/water/groundwater/explorer/index.shtml). Mean annual temperature data come from the State of Tasmania Air Temperature Logger Recording Database (© 2018 State of Tasmania), accessed through personal communication. Water quality data for the water intake station in St. Helens was provided by TasWater (pers. comm. John Fawcett).

Author Contribution

The conceptual analysis of the data presented in this paper comes from ~~LV's~~LAV's Undergraduate Honors Thesis (2020) at Eastern Michigan University. EWP, PRB, and AHS contributed to post-thesis manuscript revisions, data analysis, and figure drafting. Samples and the $^{10}Be_i$ data presented here were collected and facilitated by PRB and ECL in 2008. ^{9}Be and $^{10}Be_m$ data were first presented in Sophie E. Greene's Master's Thesis (2016) at the University of Vermont; SEG declined a request to participate in the writing and publication of this paper. AHS completed chemical weathering calculations. AJH verified Lawrence Livermore National Laboratory's measurement of beryllium at the Center for Accelerator Mass Spectrometry in 2009. This work was performed in part under the auspices of the U.S. Department of Energy by Lawrence Livermore National Laboratory under Contract DE-AC52- 07NA27344. This is LLNL-JRNL-825534.

References

ABARES, 2016, The Australian Land Use and Management Classification Version 8: Australian Bureau of Agricultural and Resource Economics and Sciences, https://www.agriculture.gov.au/abares/aclump/land-use/alum-classification.

Adams, B. A., and Ehlers, T., 2017, Deciphering topographic signals of glaciation and rock uplift in an active orogen: A case study from the Olympic Mountains, USA: Earth Surface Processes and Landforms, v. 42, no. 11, p. 1680-1692.

Aguilar, G., Carretier, S., Regard, V., Vassallo, R., Riquelme, R., and Martinod, J., 2014, Grain size-dependent 10Be concentrations in alluvial stream sediment of the Huasco Valley, a semi-arid Andes region: Quaternary Geochronology, v. 19, p. 163-172.

~~Augustinus, P., Barton, C. E., Zawadzki,~~ Aldahan, A., Haiping, Y., and Possnert, G., 1999. Distribution of beryllium between solution and minerals (biotite and albite) under atmospheric conditions and variable pH: Chemical Geology, v. 156, no. 1–4, p. 209–229.

~~A., and Harle, K., 2010, Lithological and geochemical record of mining-induced changes in sediments from Macquarie Harbour, southwest Tasmania, Australia: Environmental Earth Sciences, v. 61, no. 3, p. 625-639.~~

Balco, G., Stone, J. O., Lifton, N. A., and Dunai, T. J., 2008, A complete and easily accessible means of calculating surface exposure ages or erosion rates from 10Be and 26Al measurements: Quaternary Geochronology, v. 3, no. 3, p. 174-195.

Formatted: Left

Barreto, H. N., Varajão, C. A. C., Braucher, R., Bourlès, D. L., Salgado, A. A. R., and Varajão, A. F. D. C., 2014, The impact of diamond extraction on natural denudation rates in the Diamantina Plateau (Minas Gerais, Brazil): Journal of South American Earth Sciences, v. 56, p. 357-364.
Barrows, T. T., Stone, J. O., Fifield, L. K., and Cresswell, R. G., 2001, Late Pleistocene Glaciation of the Kosciuszko Massif, Snowy Mountains, Australia: Quaternary Research, v. 55, no. 2, p. 179-189.
-, 2002, The timing of the Last Glacial Maximum in Australia: Quaternary Science Reviews, v. 21, no. 1, p. 159-173.
Batley, G., Crawford, C., Moore, M., McNeil, J., Reid, J., Koehnken, L., and Ramsay, J., 2010, Report of the George River Water Quality Panel.
~~Beard, J., Crawford, C.,~~ ~~and Hirst, A., 2008, Developing a Monitoring Program for Six Key Estuaries in North-west Tasmania: Tasmanian Aquaculture and Fisheries Institute.~~
Belmont, P., Pazzaglia, F., and Gosse, J. C., 2007, Cosmogenic 10Be as a tracer for hillslope and channel sediment dynamics in the Clearwater River, western Washington State: Earth and Planetary Science Letters, v. 264, no. 1-2, p. 123-135.
Bierman, P., and Steig, E. J., 1996, Estimating rates of denudation using cosmogenic isotope abundances in sediment: Earth surface processes and landforms, v. 21, no. 2, p. 125-139.
Bleaney, A., Hickey, C. W., Stewart, M., Scammell, M., and Senjen, R., 2015, Preliminary investigations of toxicity in the Georges Bay catchment, Tasmania, Australia: International Journal of Environmental Studies, v. 72, no. 1, p. 1-23.
BoM, 2015, Australian Groundwater Explorer: Australia Bureau of Meteorology, http://www.bom.gov.au/water/groundwater/explorer.index.shtml.
BoM, 2021, Climate Data Online: Australia Bureau of Meteorology, http://www.bom.gov.au/climate/data/.
Braucher, R., Brown, E., Bourlès, D., and Colin, F., 2003, In situ produced 10Be measurements at great depths: implications for production rates by fast muons: Earth and Planetary Science Letters, v. 211, no. 3-4, p. 251-258.
Brown, E. T., Stallard, R. F., Larsen, M. C., Raisbeck, G. M., and Yiou, F., 1995, Denudation rates determined from the accumulation of in situ-produced 10Be in the Luquillo Experimental Forest, Puerto Rico: Earth and Planetary Science Letters, v. 129, no. 1-4, p. 193-202.
Brown, L., Pavich, M. J., Hickman, R. E., Klein, J., and Middleton, R., 1988, Erosion of the eastern United States observed with 10Be: Earth Surface Processes and Landforms, v. 13, no. 5, p. 441-457.
~~Butler, E. C., 2006, The tail of two rivers in Tasmania: the Derwent and Huon estuaries, Estuaries, Springer, p. 1-49.~~
Carretier, S., Regard, V., and Soual, C., 2009, Theoretical cosmogenic nuclide concentration in river bed load clasts: Does it depend on clast size?: Quaternary Geochronology, v. 4, no. 2, p. 108-123.
Carretier, S., Tolorza, V., Regard, V., Aguilar, G., Bermúdez, M. A., Martinod, J., Guyot, J. L., Hérail, G., and Riquelme, R., 2018, Review of erosion dynamics along the major NS climatic gradient in Chile and perspectives: Geomorphology, v. 300, p. 45-68.
Carretier, S., Tolorza, V., Rodríguez, M., Pepin, E., Aguilar, G., Regard, V., Martinod, J., Riquelme, R., Bonnet, S., and Brichau, S., 2015, Erosion in the Chilean Andes between 27 S and 39 S: tectonic, climatic and geomorphic control: Geological Society, London, Special Publications, v. 399, no. 1, p. 401-418.
Cheetham, M. D., and Martin, J. C., 2018, Hope for the best, plan for the worst: Managing sediment input in the upper catchment whilst preparing for avulsion at the mouth, 9th Australian Stream Management Conference: Hobart, Tasmania, Australia, p. 8.
Codilean, A. T., Fülöp, R.-H., Munack, H., Wilcken, K. M., Cohen, T. J., Rood, D. H., Fink, D., Bartley, R., Croke, J., and Fifield, L., 2021, Controls on denudation along the East Australian continental margin: Earth-Science Reviews, p. 103543.
Codilean, A. T., Munack, H., Cohen, T. J., Saktura, W. M., Gray, A., and Mudd, S. M., 2018, OCTOPUS: an open cosmogenic isotope and luminescence database: Earth System Science Data, v. 10, no. 4, p. 2123-2139.
Colhoun, E. A., 2002, Periglacial landforms and deposits of Tasmania : Periglacial and Permafrost Research in the Southern Hemisphere: South African Journal of Science, v. 98, no. 1, p. 55-63.
Corbett, L. B., Bierman, P. R., and Rood, D. H., 2016, An approach for optimizing in situ cosmogenic 10Be sample preparation: Quaternary Geochronology, v. 33, p. 24-34.
Cosgrove, R., 1995, Late Pleistocene behavioural variation and time trends: the case from Tasmania: Archaeology in Oceania, v. 30, no. 3, p. 83-104.

Formatted: Left

Formatted: Left

Formatted: Left

Cosgrove, R., Allen, J., and Marshall, B., 1990, Palaeo-ecology and Pleistocene human occupation in south central Tasmania: Antiquity, v. 64, no. 242, p. 59-78.

~~Coughanowr, C., and Whitehead, J., 2013, The Derwent Estuary Program: A collaborative model for science-based management, Tasmania, Australia: Ocean & Coastal Management, v. 86, p. 110-118.~~

Crawford, C., and White, C., 2005, Establishment of an integrated water quality monitoring framework for Georges Bay.

~~Creighton, C., Boon, P. I., Brookes, J. D., and Sheaves, M., 2015, Repairing Australia's estuaries for improved fisheries production—what benefits, at what cost?: Marine and Freshwater Research, v. 66, no. 6, p. 493-507.~~

Croke, J., Bartley, R., Chappell, J., Austin, J. M., Fifield, K., Tims, S. G., Thompson, C. J., and Furuichi, T., 2015, 10Be-derived denudation rates from the Burdekin catchment: The largest contributor of sediment to the Great Barrier Reef: Geomorphology, v. 241, p. 122-134.

Crowder, E., Rawlinson, N., Pilia, S., Cornwell, D. G., and Reading, A. M., 2019, Transdimensional ambient noise tomography of Bass Strait, southeast Australia, reveals the sedimentary basin and deep crustal structure beneath a failed continental rift: Geophysical Journal International, v. 217, no. 2, p. 970-987.

Dannhaus, N., Wittmann, H., Krám, P., Christl, M., and von Blanckenburg, F., 2018, Catchment-wide weathering and erosion rates of mafic, ultramafic, and granitic rock from cosmogenic meteoric 10Be/9Be ratios: Geochimica et Cosmochimica Acta, v. 222, p. 618-641.

~~Davis, J., and Kidd, I. M., 2012, Identifying Major Stressors: The Essential Precursor to Restoring Cultural Ecosystem Services in a Degraded Estuary: Estuaries and Coasts, v. 35, no. 4, p. 1007-1017.~~

Delunel, R., Schlunegger, F., Valla, P. G., Dixon, J., Glotzbach, C., Hippe, K., Kober, F., Molliex, S., Norton, K. P., Salcher, B., Wittmann, H., Akçar, N., and Christl, M., 2020, Late-Pleistocene catchment-wide denudation patterns across the European Alps: Earth-Science Reviews, v. 211, p. 103407.

Delunel, R., van der Beek, P. A., Carcaillet, J., Bourlès, D. L., and Valla, P. G., 2010, Frost-cracking control on catchment denudation rates: Insights from in situ produced 10Be concentrations in stream sediments (Ecrins–Pelvoux massif, French Western Alps): Earth and Planetary Science Letters, v. 293, no. 1-2, p. 72-83.

Deng, K., Yang, S., von Blanckenburg, F., and Wittmann, H., 2020, Denudation Rate Changes Along a Fast-Eroding Mountainous River With Slate Headwaters in Taiwan From 10Be (Meteoric)/9Be Ratios: Journal of Geophysical Research: Earth Surface, v. 125, no. 2, p. e2019JF005251.

DPIPWE, 2021, Water Information for George River at St. Helens Water Supply, Site ID 2205, Water Information Tasmania Web Portal, Tasmanian Department of Primary Industries, Parks, Water, and Environment, https://portal.wrt.tas.gov.au/Data/Location/Summary/Location/2205-1/Interval/Latest (accessed, 22 September 2021).

DPIPWE, 2021, Water Information for Ransom River at Sweets Hill, Site ID 2217, Water Information Tasmania Web Portal, Tasmanian Department of Primary Industries, Parks, Water, and Environment, https://portal.wrt.tas.gov.au/Data/Location/Summary/Location/2217-1/Interval/Latest (accessed, 22 September 2021).

Dethier, D. P., Ouimet, W., Bierman, P. R., Rood, D. H., and Balco, G., 2014, Basins and bedrock: Spatial variation in 10Be erosion rates and increasing relief in the southern Rocky Mountains, USA: Geology, v. 42, no. 2, p. 167-170.

Eppes, M.-C. and Keanini, R., 2017. Mechanical weathering and rock erosion by climate-dependent critical subcritical cracking: Review of Geophysics, v. 55, no. 2, p. 470–508.

Eppes, M.-C., Hancock, G. S., ~~Edgar, G., and Barrett, N., 2000, Effects of Catchment Activities on Macrofaunal Assemblages in Tasmanian Estuaries: Estuarine, Coastal and Shelf Science, v. 50, no. 5, p. 639-654.~~

~~Edgar, G.~~Chen, X., Arey, J., ~~Barrett, N.~~ Dewers, ,T., Huettenmoser, ~~S., Graddon, D.~~ J., Kiessling, S., Moser, F., Tannu, N., Weiserbs, B., and ~~Last, P. R., 2000, The conservation significance~~Whitten, J., 2018. Rates of ~~estuaries: a classification of Tasmanian estuaries using ecological, physical~~subcritical cracking and ~~demographic attributes as a case study: Biological Conservation~~long-term rock erosion: Geology, v. ~~92~~46, no. ~~3~~11, p. ~~383-397.~~

~~Elliott, M., Burdon, D., Hemingway, K. L., and Apitz, S. E., 2007, Estuarine, coastal and marine ecosystem restoration: confusing management and science–a revision of concepts: Estuarine, Coastal and Shelf Science, v. 74, no. 3, p. 349-366.~~

~~Ellison, J. C., and Sheehan, M.~~ 951–954~~R.,~~ ~~2014, Past, present and futures of the Tamar Estuary, Tasmania, Estuaries of Australia in 2050 and Beyond, Springer, p. 69-89~~.

Etheridge, M. A., Branson, J. C., and Stuart-Smith, P. G., 1987, The Bass, Gippsland and Otway basins, southeast Australia: A branched rift system formed by continental extension: Sedimentary Basins and Basin-forming Mechanisms, v. Memoir 12, p. 147-162.

Formatted: Left

Formatted: Left

Formatted: Left

Formatted: Left

Formatted: Left

Fellin, M. G., Chen, C.-Y., Willett, S. D., Christl, M., and Chen, Y.-G., 2017, Erosion rates across space and timescales from a multi-proxy study of rivers of eastern Taiwan: Global and Planetary Change, v. 157, p. 174-193.

Ferrier, K. L., Kirchner, J. W., and Finkel, R. C., 2005, Erosion rates over millennial and decadal timescales at Caspar Creek and Redwood Creek, northern California Coast Ranges: Earth Surface Processes and Landforms: The Journal of the British Geomorphological Research Group, v. 30, no. 8, p. 1025-1038.

Fick, S. E., and Hijmans, R. J., 2017, WorldClim 2: new 1-km spatial resolution climate surfaces for global land areas: International Journal of Climatology, v. 37, no. 12, p. 4302-4315.

~~Fitzsimons, J. A., Hale, L., Hancock, B., and Beck, M. W., 2015, Developing a marine conservation program in temperate Australia: determining priorities for action: Australian Journal of Maritime & Ocean Affairs, v. 7, no. 1, p. 85-93.~~

Foster, D. A., and Gray, D. R., 2000, Evolution and Structure of the Lachlan Fold Belt (Orogen) of Eastern Australia: Annual Review of Earth and Planetary Sciences, v. 28, no. 1, p. 47-80.

Fülöp, R.-H., Codilean, A. T., Wilcken, K. M., Cohen, T. J., Fink, D., Smith, A. M., Yang, B., Levchenko, V. A., Wacker, L., Marx, S. K., Stromsoe, N., Fujioka, T., and Dunai, T. J., 2020, Million-year lag times in a post-orogenic sediment conveyor: Science Advances, v. 6, no. 25, p. eaaz8845.

Gaina, C., Müller, D. R., Royer, J.-Y., Stock, J., Hardebeck, J., and Symonds, P., 1998, The tectonic history of the Tasman Sea: A puzzle with 13 pieces: Journal of Geophysical Research: Solid Earth, v. 103, no. B6, p. 12413-12433.

Gallant, J., Wilson, N., Dowling, T., Read, A., and Inskeep, C., 2011, SRTM-derived 1 Second Digital Elevation Models Version 1.0. Record 1: Geoscience Australia, Canberra, ACT, Australia.

Gee, R. D., and Groves, D. I., 1971, Structural features and mode of emplacement of part of the blue tier batholith in Northeast Tasmania: Journal of the Geological Society of Australia, v. 18, no. 1, p. 41-55.

~~Geist, J., and Hawkins, S. J., 2016, Habitat recovery and restoration in aquatic ecosystems: current progress and future challenges: Aquatic Conservation: Marine and Freshwater Ecosystems, v. 26, no. 5, p. 942-962.~~

Godard, V., Dosseto, A., Fleury, J., Bellier, O., and Siame, L., 2019, Transient landscape dynamics across the Southeastern Australian Escarpment: Earth and Planetary Science Letters, v. 506, p. 397-406.

Gonzalez, V. S., Bierman, P. R., Nichols, K. K., and Rood, D. H., 2016, Long-term erosion rates of Panamanian drainage basins determined using in situ 10Be: Geomorphology, v. 275, p. 1-15.

Gosse, J. C., and Phillips, F. M., 2001, Terrestrial in situ cosmogenic nuclides: theory and application: Quaternary Science Reviews, v. 20, no. 14, p. 1475-1560.

Graly, J. A., Bierman, P. R., Reusser, L. J., and Pavich, M. J., 2010, Meteoric 10Be in soil profiles – A global meta-analysis: Geochimica et Cosmochimica Acta, v. 74, no. 23, p. 6814-6829.

Graly, J. A., Reusser, L. J., and Bierman, P. R., 2011, Short and long-term delivery rates of meteoric 10Be to terrestrial soils: Earth and Planetary Science Letters, v. 302, no. 3, p. 329-336.

Grande, A., Schmidt, A. H., Bierman, P. R., Corbett, L. B., López-Lloreda, C., Willenbring, J., McDowell, W. H., and Caffee, M. W., 2021, Landslides, hurricanes, and sediment sourcing impact basin-scale erosion estimates in Luquillo, Puerto Rico: Earth and Planetary Science Letters, v. 562, p. 116821.

Granger, D. E., Kirchner, J. W., and Finkel, R., 1996, Spatially averaged long-term erosion rates measured from in situ-produced cosmogenic nuclides in alluvial sediment: The Journal of Geology, v. 104, no. 3, p. 249-257.

Gray, D. R., and Foster, D. A., 2004, Tectonic evolution of the Lachlan Orogen, southeast Australia: Historical review, data synthesis and modern perspectives: Australian Journal of Earth Sciences, v. 51, no. 6, p. 773-817.

Greene, E. S., 2016, Comparing meteoric 10Be, in situ 10Be, and native 9Be across a diverse set of watersheds, Master's Thesis, Geology Department, University of Vermont, Burlington, VT, United States, 118 p.

Griffiths, J. R., 1971, Continental margin tectonics and the evolution of south-east Australia: The APPEA Journal, v. 11, no. 1, p. 75-79.

Gunn, P. J., 1975, Mesozoic-Cainozoic Tectonics and Igneous Activity: Southeastern Australia: Journal of the Geological Society of Australia, v. 22, no. 2, p. 215-221.

~~Hancock, G., and Kirwan, M., 2007, Summit erosion rates deduced from 10Be: Implications for relief production in the central Appalachians: Geology, v. 35, no. 1, p. 89-92.~~

Hales, T. C. and Roering, J. J., 2006. Climatic controls on frost cracking and implications for the evolution of bedrock landscapes: Journal of Geophysical Research, v. 11, F02033.

Formatted: Left

Formatted: Left

Harel, M.-A., Mudd, S., and Attal, M., 2016, Global analysis of the stream power law parameters based on worldwide 10Be denudation rates: Geomorphology, v. 268, p. 184-196.
Harrison, E. J., Willenbring, J. K., and Brocard, G. Y., 2021, Quaternary record of terrestrial environmental change in response to climatic forcing and anthropogenic perturbations, in Puerto Rico: Quaternary Science Reviews, v. 253, p. 106770.
Hayes, D. E., and Ringis, J., 1973, Seafloor Spreading in the Tasman Sea: Nature, v. 243, no. 5408, p. 454-458.
Heikkilä, U., and von Blanckenburg, F., 2015, The global distribution of Holocene meteoric 10Be fluxes from atmospheric models. Distribution maps for terrestrial Earth's surface applications, GFZ Data Services, doi.10.5880/GFZ.3.4.2015.001
Heisinger, B., Niedermayer, M., Hartmann, F., Korschinek, G., Nolte, E., Morteani, G., Neumaier, S., Petitjean, C., Kubik, P., and Synal, A., 1997, In-situ production of radionuclides at great depths: Nuclear Instruments and Methods in Physics Research Section B: Beam Interactions with Materials and Atoms, v. 123, no. 1-4, p. 341-346.
Helz, G. R., and Valette-Silver, N., 1992, Beryllium-10 in Chesapeake Bay sediments: An indicator of sediment provenance: Estuarine, Coastal and Shelf Science, v. 34, no. 5, p. 459-469.
Henck, A. C., Huntington, K. W., and Hallet, B., 2011. Spatial controls on erosion in the Three Rivers Region, southwest China: Earth and Planetary Science Letters, v. 303, p. 71–83.
Higgins, N. C., Solomon, M., and Varne, R., 1985, The genesis of the Blue Tier Batholith, northeastern Tasmania, Australia: Lithos, v. 18, p. 129-149.
Huffman, G., Pendergrass, J., and Angeline & National Center for Atmospheric Research Staff (Eds.), 2021. The Climate Data Guide: TRMM: Tropical Rainfall Measuring Mission: Last modified 20 Mar 2021. Retrieved from https://climatedataguide.ucar.edu/climate-data/trmm-tropical-rainfall-measuring-mission.
Jerie, K., Houshold, I., and Peters, D., 2003, Tasmania's river geomorphology: stream character and regional analysis: Nature Conservation Branch, DPIWE.
Jones, B., Chenhall, B., Debretsion, F., and Hutton, A., 2003, Geochemical comparisons between estuaries with non-industrialised and industrialised catchments: The Huon and Derwent River estuaries, Tasmania: Australian Journal of Earth Sciences, v. 50, no. 5, p. 653-667.
Jones, P. J., Williamson, G. J., Bowman, D. M. J. S., Lefroy, E. C., 2019, Mapping Tasmania's cultural landscapes: Using habitat suitability modelling of archaeological sites as a landscape history tool: Journal of Biogeography, v. 46, no. 11, p. 2570-2582.
Jungers, M. C., Bierman, P. R., Matmon, A., Nichols, K., Larsen, J., and Finkel, R., 2009, Tracing hillslope sediment production and transport with in situ and meteoric ^{10}Be: Journal of Geophysical Research, v. 114, F04020.
Kidd, D., Malone, B., McBratney, A., Minasny, B., Odgers, N., Webb, M., and Searle, R., 2014, A new digital soil resource for Tasmania, Australia, in Proceedings 20th World Congress of Soil Science, p. 612-613.
Kidd, D., Webb, M., Malone, B., Minasny, B., and McBratney, A., 2015, 80-metre resolution 3D soil attribute maps for Tasmania, Australia: Soil Research, doi. 10.1071/SR14268.
Knighton, A., 1991, Channel bed adjustment along mine-affected rivers of northeast Tasmania: Geomorphology, v. 4, no. 3-4, p. 205-219.
Koehnken, L., 2001, North-east rivers environmental review: A review of Tasmanian environmental quality data to 2001: Supervising Scientist Report 168, Australian Government Department of Agriculture, Water and the Environment, pp. 64.
Kohl, C. P., and Nishiizumi, K., 1992, Chemical isolation of quartz for measurement of in-situ -produced cosmogenic nuclides: Geochimica et Cosmochimica Acta, v. 56, no. 9, p. 3583-3587.
Kohn, B. P., Gleadow, A. J. W., Brown, R. W., Gallagher, K., O'Sullivan, P. B., and Foster, D. A., 2002, Shaping the Australian crust over the last 300 million years: Insights from fission track thermotectonic imaging and denudation studies of key terranes: Australian Journal of Earth Sciences, v. 49, no. 4, p. 697-717.
Kottek, M., Grieser, J., Beck, C., Rudolf, B., and Rubel, F., 2006, World map of the Köppen-Geiger climate classification updated: Meteorologische Zeitschrift, v. 15, no. 3, p. 259-263.
Kragt, M. E., and Newham, L. T., 2009, Developing a water-quality model for the George catchment, Tasmania: Landscape Logic.

Formatted: Left
Formatted: Left
Formatted: Left
Formatted: Left
Formatted: Left
Formatted: Left

Lal, D., 1991, Cosmic ray labeling of erosion surfaces: in situ nuclide production rates and erosion models: Earth and Planetary Science Letters, v. 104, no. 2-4, p. 424-439.

Land-Tasmania, 2020, Fire History [of Tasmania]: Tasmania Department of Primary Industries, Water and Environment, Hobart, Tasmania, Australia, https://www.thelist.tas.gov.au/app/content/data/geo-meta-data-record?detailRecordUID=b94d4388-995d-416a-9844-a39de2798bed.

Lanyon, R., Varne, R., and Crawford, A. J., 1993, Tasmanian Tertiary basalts, the Balleny plume, and opening of the Tasman Sea (southwest Pacific Ocean): Geology, v. 21, no. 6, p. 555-558.

Mackintosh, A. N., Barrows, T. T., Colhoun, E. A., and Fifield, L. K., 2006, Exposure dating and glacial reconstruction at Mt. Field, Tasmania, Australia, identifies MIS 3 and MIS 2 glacial advances and climatic variability: Journal of Quaternary Science, v. 21, no. 4, p. 363-376.

~~Marshall, J. A., Roering, J. J., Gavin, D. G., and Granger, D. E., 2017, Late Quaternary climatic controls on erosion rates and geomorphic processes in western Oregon, USA: GSA Bulletin, v. 129, no. 5-6, p. 715-731.~~

Martin, J., and Cheetham, M., 2018, Final Report: Lower George River Investigation: Lower George Riverworks Trust.

~~Martin-Smith, K. M., and Vincent, A. C., 2005, Seahorse declines in the Derwent estuary, Tasmania in the absence of fishing pressure: Biological Conservation, v. 123, no. 4, p. 533-545.~~

Masarik, J., and Beer, J., 2009, An updated simulation of particle fluxes and cosmogenic nuclide production in the Earth's atmosphere: Journal of Geophysical Research: Atmospheres, v. 114, no. D11.

Matmon, A., Bierman, P., and Enzel, Y., 2002, Pattern and tempo of great escarpment erosion: Geology, v. 30, no. 12, p. 1135-1138.

McCarthy, T. S., and Groves, D. I., 1979, The Blue Tier Batholith, Northeastern Tasmania: Contributions to Mineralogy and Petrology, v. 71, no. 2, p. 193-209.

McDougall, I., and van der Lingen, G. J., 1974, Age of the rhyolites of the Lord Howe Rise and the evolution of the southwest Pacific Ocean: Earth and Planetary Science Letters, v. 21, no. 2, p. 117-126.

McIntosh, P. D., Price, D. M., Eberhard, R., and Slee, A. J., 2009, Late Quaternary erosion events in lowland and mid-altitude Tasmania in relation to climate change and first human arrival: Quaternary Science Reviews, v. 28, no. 9, p. 850-872.

McKenny, C., and Shepherd, C., 1999, Ecological flow requirements for the George River: Report Series WRA 99/14, Department of Primary Industries, Water and Environment, Tasmania, pp. 31.

Mishra, A. K., Placzek, C., and Jones, R., 2019, Coupled influence of precipitation and vegetation on millennial-scale erosion rates derived from 10Be: PloS one, v. 14, no. 1, p. e0211325.

Mitchell, I. M., Crawford, C. M., and Rushton, M. J., 2000, Flat oyster (Ostrea angasi) growth and survival rates at Georges Bay, Tasmania (Australia): Aquaculture, v. 191, no. 4, p. 309-321.

Monaghan, M. C., Krishnaswami, S., and Turekian, K. K., 1986, The global-average production rate of10Be: Earth and Planetary Science Letters, v. 76, no. 3, p. 279-287.

Mortimer, N., Campbell, H. J., Tulloch, A. J., King, P. R., Stagpoole, V. M., Wood, R. A., Rattenbury, M. S., Sutherland, R., Adams, C. J., Collot, J., and Seton, M., 2017, Zealandia: Earth's hidden continent: GSA Today, v. 27, p. 27-35.

Mount, R., Crawford, C., Veal, C., and White, C., 2005, Bringing back the bay: marine habitats and water quality in Georges Bay.

~~Murphy, R., Crawford, C., and Barmuta, L., 2003, Estuarine Health in Tasmania, Status and Indicators: Water Quality: Tasmanian Aquaculture and Fisheries Institute.~~

~~Nanson, G. C., Von Krusenstierna, A., Bryant, E. A., and Renilson, M. R., 1994, Experimental measurements of river-bank erosion caused by boat-generated waves on the gordon river, Tasmania: Regulated Rivers: Research & Management, v. 9, no. 1, p. 1-14.~~

Neilson, T. B., Schmidt, A. H., Bierman, P. R., Rood, D. H., and Sosa Gonzalez, V., 2017, Efficacy of in situ and meteoric 10Be mixing in fluvial sediment collected from small catchments in China: Chemical Geology, v. 471, p. 119-130.

Nichols, K. K., Bierman, P. R., and Rood, D. H., 2014, 10Be constrains the sediment sources and sediment yields to the Great Barrier Reef from the tropical Barron River catchment, Queensland, Australia: Geomorphology, v. 224, p. 102-110.

Niemi, N. A., Oskin, M., Burbank, D. W., Heimsath, A. M., and Gabet, E. J., 2005, Effects of bedrock landslides on cosmogenically determined erosion rates: Earth and Planetary Science Letters, v. 237, no. 3, p. 480-498.

Formatted: Left

Formatted: Left

Formatted: Left

Nishiizumi, K., Imamura, M., Caffee, M. W., Southon, J. R., Finkel, R. C., and McAninch, J., 2007, Absolute calibration of 10Be AMS standards: Nuclear Instruments and Methods in Physics Research Section B: Beam Interactions with Materials and Atoms, v. 258, no. 2, p. 403-413.

Noe, G. B., Cashman, M. J., Skalak, K., Gellis, A., Hopkins, K. G., Moyer, D., Webber, J., Benthem, A., Maloney, K., and Brakebill, J., 2020, Sediment dynamics and implications for management: State of the science from long-term research in the Chesapeake Bay watershed, USA: Wiley Interdisciplinary Reviews: Water, v. 7, no. 4, p. e1454.

Persano, C., Stuart, F. M., Bishop, P., and Barfod, D. N., 2002, Apatite (U–Th)/He age constraints on the development of the Great Escarpment on the southeastern Australian passive margin: Earth and Planetary Science Letters, v. 200, no. 1, p. 79-90.

Portenga, E. W., and Bierman, P. R., 2011, Understanding Earth's eroding surface with 10 Be: GSA Today, v. 21, no. 8, p. 4-10.

Portenga, E. W., Bierman, P. R., Duncan, C., Corbett, L. B., Kehrwald, N. M., and Rood, D. H., 2015, Erosion rates of the Bhutanese Himalaya determined using in situ-produced 10Be: Geomorphology, v. 233, p. 112-126.

Portenga, E. W., Bierman, P. R., Trodick, C. D., Jr., Greene, S. E., DeJong, B. D., Rood, D. H., and Pavich, M. J., 2019, Erosion rates and sediment flux within the Potomac River basin quantified over millennial timescales using beryllium isotopes: GSA Bulletin, v. 131, no. 7-8, p. 1295-1311.

Portenga, E. W., Bishop, P., Rood, D. H., and Bierman, P. R., 2017, Combining bulk sediment OSL and meteoric 10Be fingerprinting techniques to identify gully initiation sites and erosion depths: Journal of Geophysical Research: Earth Surface, v. 122, no. 2, p. 513-527.

Preston, K., 2012, Anchor tin mine, Tasmania: A century of struggle for profitability, Australasian Mining History Association, v. 10, p. 140–159.

Puchol, N., Lavé, J., Lupker, M., Blard, P.-H., Gallo, F., and France-Lanord, C., 2014, Grain-size dependent concentration of cosmogenic 10Be and erosion dynamics in a landslide-dominated Himalayan watershed: Geomorphology, v. 224, p. 55-68.

Rahaman, W., Wittmann, H., and von Blanckenburg, F., 2017, Denudation rates and the degree of chemical weathering in the Ganga River basin from ratios of meteoric cosmogenic 10Be to stable 9Be: Earth and Planetary Science Letters, v. 469, p. 156-169.

Reusser, L., Graly, J., Bierman, P., and Rood, D., 2010a, Calibrating a long-term meteoric 10Be accumulation rate in soil: Geophysical Research Letters, v. 37, no. 19.

Reusser, L. J., and Bierman, P. R., 2010, Using meteoric 10Be to track fluvial sand through the Waipaoa River basin, New Zealand: Geology, v. 38, no. 1, p. 47-50.

Rosenkranz, R., Schildgen, T., Wittmann, H., and Spiegel, C., 2018, Coupling erosion and topographic development in the rainiest place on Earth: Reconstructing the Shillong Plateau uplift history with in-situ cosmogenic 10Be: Earth and Planetary Science Letters, v. 483, p. 39-51.

Schaller, M., Blanckenburg, F. v., Hovius, N., Veldkamp, A., van den Berg, M. W., and Kubik, P., 2004, Paleoerosion rates from cosmogenic 10Be in a 1.3 Ma terrace sequence: response of the River Meuse to changes in climate and rock uplift: The Journal of geology, v. 112, no. 2, p. 127-144.

Schaller, M., Ehlers, T., Lang, K. A., Schmid, M., and Fuentes-Espoz, J., 2018, Addressing the contribution of climate and vegetation cover on hillslope denudation, Chilean Coastal Cordillera (26–38 S): Earth and Planetary Science Letters, v. 489, p. 111-122.

Schaller, M., Ehlers, T., Stor, T., Torrent, J., Lobato, L., Christl, M., and Vockenhuber, C., 2016, Spatial and temporal variations in denudation rates derived from cosmogenic nuclides in four European fluvial terrace sequences: Geomorphology, v. 274, p. 180-192.

Schaller, M., von Blanckenburg, F., Hovius, N., and Kubik, P., 2001, Large-scale erosion rates from in situ-produced cosmogenic nuclides in European river sediments: Earth and Planetary Science Letters, v. 188, no. 3-4, p. 441-458.

Scherler, D., Bookhagen, B., and Strecker, M. R., 2014, Tectonic control on 10Be-derived erosion rates in the Garhwal Himalaya, India: Journal of Geophysical Research: Earth Surface, v. 119, no. 2, p. 83-105.

Schmidt, A. H., Gonzalez, V. S., Bierman, P. R., Neilson, T. B., and Rood, D. H., 2018, Agricultural land use doubled sediment loads in western China's rivers: Anthropocene, v. 21, p. 95-106.

Formatted: Left

Formatted: Left

Formatted: Left

Schmidt, A. H., Neilson, T. B., Bierman, P. R., Rood, D. H., Ouimet, W. B., and Sosa Gonzalez, V., 2016, Influence of topography and human activity on apparent in situ 10Be-derived erosion rates in Yunnan, SW China: Earth Surf. Dynam., v. 4, no. 4, p. 819-830.

~~Seen, A., Townsend, A., Atkinson, B., Ellison, J., Harrison, J., and Heijnis, H., 2004, Determining the History and Sources of Contaminants in Sediments in the Tamar Estuary, Tasmania, Using 210Pb Dating and Stable Pb Isotope Analyses: Environmental Chemistry, v. 1, no. 1, p. 49-54.~~

Seymour, D. B., Green, G. R., and Calver, C. R., 2006, The geology and mineral deposits of Tasmania: A summary: Mineral Resources Tasmania, https://www.mrt.tas.gov.au/products/publications/the_geology_and_mineral_deposits_of_tasmania_a_summary.

Siame, L., Angelier, J., Chen, R.-F., Godard, V., Derrieux, F., Bourlès, D., Braucher, R., Chang, K.-J., Chu, H.-T., and Lee, J.-C., 2011, Erosion rates in an active orogen (NE-Taiwan): A confrontation of cosmogenic measurements with river suspended loads: Quaternary Geochronology, v. 6, no. 2, p. 246-260.

Singleton, A. A., Schmidt, A. H., Bierman, P. R., Rood, D. H., Neilson, T. B., Greene, E. S., Bower, J. A., Perdrial, N., 2016, Effects of grain size, mineralogy, and acid-extractable grain coatings on the distribution of the fallout radionuclides ^{7}Be, ^{10}Be, ^{137}Cs, and ^{210}Pb in river sediment: Geochimica et Cosmochimica Acta, v. 197, p. 71-86.

Starke, J., Ehlers, T., and Schaller, M., 2017, Tectonic and climatic controls on the spatial distribution of denudation rates in Northern Chile (18 S to 23 S) determined from cosmogenic nuclides: Journal of Geophysical Research: Earth Surface, v. 122, no. 10, p. 1949-1971.

-, 2020, Latitudinal effect of vegetation on erosion rates identified along western South America: Science, v. 367, no. 6484, p. 1358-1361.

Stone, J., 1998, A Rapid Fusion Method for Separation of Beryllium-10 From Soils and Silicates: Geochimica et Cosmochimica Acta, v. 62, no. 3, p. 555-561.

-, 2000. Air pressure and cosmogenic isotope production: Journal of Geophysical Research, v. 105, no. B10, p. 23,753–23,759.

Sutherland, R., King, P., and Wood, R., 2001, Tectonic evolution of Cretaceous rift basins in south-eastern Australia and New Zealand: Implications for exploration risk assessment, Petroleum Exploration Society of Australia Eastern Australasian Basins Symposium: Melbourne, Victoria, Australia.

Tomkins, K. M., Humphreys, G. S., Wilkinson, M. T., Fink, D., Hesse, P. P., Doerr, S. H., Shakesby, R. A., Wallbrink, P. J., and Blake, W. H., 2007, Contemporary versus long-term denudation along a passive plate margin: the role of extreme events: Earth Surface Processes and Landforms, v. 32, no. 7, p. 1013-1031.

Valette-Silver, J. N., Brown, L., Pavich, M., Klein, J., and Middleton, R., 1986, Detection of erosion events using10Be profiles: example of the impact of agriculture on soil erosion in the Chesapeake Bay area (U.S.A.): Earth and Planetary Science Letters, v. 80, no. 1, p. 82-90.

van Dongen, R., Scherler, D., Wittmann, H., and von Blanckenburg, F., 2019, Cosmogenic 10Be in river sediment: where grain size matters and why: Earth Surf. Dynam., v. 7, no. 2, p. 393-410.

van Geen, A., Valette-Silver, N. J., Luoma, S. N., Fuller, C. C., Baskaran, M., Tera, F., and Klein, J., 1999, Constraints on the sedimentation history of San Francisco Bay from 14C and 10Be: Marine Chemistry, v. 64, no. 1, p. 29-38.

Vanacker, V., von Blanckenburg, F., Govers, G., Molina, A., Poesen, J., Deckers, J., and Kubik, P., 2007, Restoring dense vegetation can slow mountain erosion to near natural benchmark levels: Geology, v. 35, no. 4, p. 303-306.

~~Verdonschot, P., Spears, B., Feld, C., Brucet, S., Keizer-Vlek, H., Borja, A., Elliott, M., Kernan, M., and Johnson, R., 2013, A comparative review of recovery processes in rivers, lakes, estuarine and coastal waters: Hydrobiologia, v. 704, no. 1, p. 453-474.~~

von Blanckenburg, F., Bouchez, J., and Wittmann, H., 2012, Earth surface erosion and weathering from the 10Be (meteoric)/9Be ratio: Earth and Planetary Science Letters, v. 351-352, p. 295-305.

Webb, M. A., Kidd, D., and Minasny, B., 2020. Near real-time mapping of air temperature at high spatiotemporal resolutions in Tasmania, Australia: Theoretical and Applied Climatology, v. 141, p. 1181–1201.

Webb, M., Pirie, A., Kidd, D., and Minasny, B., 2018, Spatial analysis of frost risk to determine viticulture suitability in Tasmania, Australia: Australian Journal of Grape and Wine Research, v. 24, no. 2, 219–233.

Weissel, J. K., and Hayes, D. E., 1977, Evolution of the Tasman Sea reappraised: Earth and Planetary Science Letters, v. 36, no. 1, p. 77-84.

Formatted: Left

Formatted: Left

Formatted: Left

Formatted: Left

Formatted: Left

West, A. J., Galy, A., and Bickle, M., 2005, Tectonic and climatic controls on silicate weathering: Earth and Planetary Science Letters, v. 235, p. 211–228.
Wilford, J., Searle, R., Thomas, M., Pagendam, D. E., and Grundy, M., 2016. A regolith depth map of the Australian continent: Geoderma, v. 266, p. 1–13.
Willenbring, J. K., and von Blanckenburg, F., 2010, Meteoric cosmogenic Beryllium-10 adsorbed to river sediment and soil: Applications for Earth-surface dynamics: Earth-Science Reviews, v. 98, no. 1, p. 105-122.
Wilson, C. J., 1999, Effects of logging and fire on runoff and erosion on highly erodible granitic soils in Tasmania: Water Resources Research, v. 35, no. 11, p. 3531-3546.
Wittmann, H., Malusà, M. G., Resentini, A., Garzanti, E., and Niedermann, S., 2016, The cosmogenic record of mountain erosion transmitted across a foreland basin: Source-to-sink analysis of in situ 10Be, 26Al and 21Ne in sediment of the Po river catchment: Earth and Planetary Science Letters, v. 452, p. 258-271.
Wittmann, H., Oelze, M., Gaillardet, J., Garzanti, E., and von Blanckenburg, F., 2020, A global rate of denudation from cosmogenic nuclides in the Earth's largest rivers: Earth-Science Reviews, v. 204, p. 103147.
Wittmann, H., von Blanckenburg, F., Bouchez, J., Dannhaus, N., Naumann, R., Christl, M., and Gaillardet, J., 2012, The dependence of meteoric 10Be concentrations on particle size in Amazon River bed sediment and the extraction of reactive 10Be/9Be ratios: Chemical Geology, v. 318-319, p. 126-138.
Wittmann, H., von Blanckenburg, F., Dannhaus, N., Bouchez, J., Gaillardet, J., Guyot, J. L., Maurice, L., Roig, H., Filizola, N., and Christl, M., 2015, A test of the cosmogenic 10Be(meteoric)/9Be proxy for simultaneously determining basin-wide erosion rates, denudation rates, and the degree of weathering in the Amazon basin: Journal of Geophysical Research: Earth Surface, v. 120, no. 12, p. 2498-2528.
Wittmann, H., von Blanckenburg, F., Guyot, J.-L., Maurice, L., and Kubik, P., 2011, Quantifying sediment discharge from the Bolivian Andes into the Beni foreland basin from cosmogenic 10Be-derived denudation rates: Revista Brasileira de Geociências, v. 41, no. 4, p. 629-641.
Wittmann, H., von Blanckenburg, F., Guyot, J. L., Maurice, L., and Kubik, P. W., 2009, From source to sink: Preserving the cosmogenic 10Be-derived denudation rate signal of the Bolivian Andes in sediment of the Beni and Mamoré foreland basins: Earth and Planetary Science Letters, v. 288, no. 3, p. 463-474.
~~Wolanski, E., and Ducrotoy, J. P., 2014, Estuaries of Australia in 2050 and beyond–A synthesis, Estuaries of Australia in 2050 and beyond, Springer, p. 1-13.~~
Yanites, B. J., Tucker, G. E., and Anderson, R. S., 2009, Numerical and analytical models of cosmogenic radionuclide dynamics in landslide-dominated drainage basins: Journal of Geophysical Research: Earth Surface, v. 114, no. F1.
You, C.F., Lee, T., and Li, Y.H., 1989. The partition of Be between soil and water: Chemical Geology, v. 77, p. 105–118.

Formatted: Left

Formatted: Font color: Custom Color(RGB(34,34,34))

Formatted: Left, Indent: Left: 0", First line: 0", Line spacing: 1.5 lines